UM-AC 93-15

A QUANTITATIVE ANALYSIS OF IRAS MAPS OF MOLECULAR CLOUDS

Jennifer J. Wiseman
Harvard-Smithsonian Center for Astrophysics

and

Fred C. Adams
University of Michigan

A QUANTITATIVE ANALYSIS OF IRAS MAPS OF MOLECULAR CLOUDS

Jennifer J. Wiseman[1] and Fred C. Adams[2]

[1] *Harvard-Smithsonian Center for Astrophysics*
60 Garden Street, Cambridge, MA 02138

[2] *Physics Department, University of Michigan*
Ann Arbor, MI 48109

submitted to the Astrophysical Journal: 17 September 1993
revised: 1 April 1994

Abstract

We present an analysis of *IRAS* maps of five molecular clouds: Orion, Ophiuchus, Perseus, Taurus, and Lupus. For the classification and description of these astrophysical maps, we use a newly developed technique which considers all maps of a given type to be elements of a pseudometric space. For each physical characteristic of interest, this formal system assigns a distance function (a pseudometric) to the space of all maps; this procedure allows us to measure quantitatively the difference between any two maps and to order the space of all maps. We thus obtain a quantitative classification scheme for molecular clouds. In this present study we use the *IRAS* continuum maps at 100μm and 60μm to produce column density (or optical depth) maps for the five molecular cloud regions given above. For this sample of clouds, we compute the "output" functions which measure the distribution of density, the distribution of topological components, the self-gravity, and the filamentary nature of the clouds. The results of this work provide a quantitative description of the structure in these molecular cloud regions. We then order the clouds according to the overall environmental "complexity" of these star forming regions. Finally, we compare our results with the observed populations of young stellar objects in these clouds and discuss the possible environmental effects on the star formation process. Our results are consistent with the recently stated conjecture that more massive stars tend to form in more "complex" environments.

Subject headings: interstellar: molecules – stars: formation – methods: analytical – methods: data analysis

1. INTRODUCTION

Molecular clouds are important constituents of the galaxy and comprise a substantial fraction of the galactic mass. The study of molecular clouds is important on two conceptually different levels: Molecular clouds can be considered as astrophysical objects in their own right and therefore studied as evolving astrophysical systems. On the other hand, these clouds can be considered as providing the initial conditions and background environment for the star formation process. This present study has two coupled goals: (1) We want to provide a classification scheme for molecular clouds. (2) We want to begin a quantitative study of the environmental effects on star formation. In a companion paper (Adams & Wiseman 1994; hereafter AW), we extend the existing formal techniques for the analysis and classification of astrophysical maps in general.

Although molecular clouds are extremely well studied objects and a wealth of observational data exists, quantitative analyses of these clouds are just now being done. For example, many authors have tried to ascertain the degree to which molecular clouds are fractals (e.g., Bazell & Désert 1988; Dickman, Horvath, & Margulis 1990; Falgarone, Phillips, & Walker 1991). Veeraraghavan & Fuller (1991) have applied techniques from the study of large scale structure in the universe (see Gott, Melott, & Dickinson 1986) to the study of molecular clouds. Houlahan & Scalo (1992) have studied molecular cloud structure using a "tree" algorithm which represents a large molecular cloud map as a "data tree" (see also Scalo 1990); this method explicitly searches for hierarchical structure in the clouds. Stenholm (1990) has studied molecular clouds by using a statistical analysis of the properties of molecular line profiles in the maps.

Many studies have focused on defining "clumps" in molecular clouds and finding the clump mass spectrum (see, e.g., Bally et al. 1987; Carr 1987; Loren 1989; Lada, Bally, & Stark 1991; Stutzki & Gusten 1990; and the review of Blitz 1993). Langer, Wilson, & Anderson (1993) have recently completed a wavelet analysis of interstellar clouds and have found a clump mass spectrum of the form $dN/dM \sim M^{-5/3}$ for the cloud Barnard 5 (they also find evidence for hierarchical structure). Using a different procedure, Williams, de Geus, & Blitz (1994) have found the clump mass spectrum for both the Maddalena molecular cloud (which has an abnormally low level of star formation compared to other molecular clouds) and the Rosette molecular cloud (a more typical star forming cloud). Both clouds have similar cloud mass spectra $dN/dM \sim M^{-p}$, where $p = 1.32$ for the Rosette cloud and $p = 1.44$ for the Maddalena cloud. To summarize, molecular clouds seem to exhibit clump mass spectra of the form $dN/dM \sim M^{-p}$, where $p \approx 3/2$ is a rather robust value.

Another useful approach to describing molecular cloud structure is to consider the cloud's overall "complexity". Myers (1991) has given a qualitative description of several nearby molecular cloud complexes; he suggests that these star forming regions can be ordered according to their "complexity" and that the environment can affect the nature of the stars forming within these clouds. Recently, Wood, Myers, & Daugherty (1994; hereafter WMD) have used this same approach to study *IRAS* maps of molecular clouds. Our present analysis is both a complement and an extension of the work of Myers (1991) and WMD; we provide a quantitative description and determination of "complexity" and

other relevant environmental factors which may influence the star formation process.

In order to provide a classification scheme for molecular clouds, we must be able to measure the difference between any two clouds and to order a set of clouds in some physically meaningful manner. Unfortunately, the science of form description for complex irregular entities (such as the molecular clouds in this study) remains poorly developed (Lord & Wilson 1984). In this paper, we utilize a new formalism (Adams 1992; hereafter Paper I) which considers the difference between any two clouds to be the "distance" between two elements of a metric space (here, the space of all molecular clouds). We then proceed by constructing distance functions (here, pseudometrics) for the space (see our companion paper AW and Paper I for further details regarding this formalism). As we illustrate in this paper, this method of form description provides an effective means of classifying molecular cloud maps.

The results of this present analysis of molecular clouds allows us (in principle) to test speculations concerning environmental effects on the star formation process (see, e.g., Shu, Adams, & Lizano 1987 for a general review; see also Lada & Shu 1990). For example, one important unsettled issue is the question of bimodal star formation, i.e., the assertion that high-mass stars form in different environments than low-mass stars (see, e.g., Herbig 1962; Mezger & Smith 1977; see also Zinnecker, McCaughrean, & Wilking 1993 for a recent review). In order to address this question, we must first be able to quantitatively describe "different environments" for star formation. The results of this paper provide such a description. However, the other half of the problem – a description of the populations of young stellar objects in the clouds – remains poorly determined (largely due to observational selection). As another example, the current theory of star formation considers molecular cloud cores (the actual sites of star formation) to be isolated and nearly spherical in shape. This theoretical idealization of a star forming site has been remarkably successful in predicting many properties of protostellar objects (see, e.g., the review of Shu et al. 1987) and has a well-defined and calculable signature in the method of form description used here. We can thus test how well actual star forming regions fit this theoretical idealization (see §4).

This paper is organized as follows. We define the observational sample of molecular clouds in §2. In §3, we review the formalism for measuring the distance between molecular clouds and ordering the space of all clouds. In §4 we calculate output functions for the clouds in our sample and use the results to determine coordinates for the clouds. Using these results, we order the set of clouds according to each physical characteristic of interest. In §5, we discuss the observed populations of young stellar objects in these clouds and discuss their relationship with the cloud characteristics as described in this paper. We conclude in §6 with a discussion and summary of our results.

2. THE MAPS

For our sample of molecular clouds, we use maps of column density (or, equivalently, optical depth) constructed from the *IRAS* all-sky survey. Our sample includes five "well-known" molecular cloud regions: Orion, Ophiuchus, Taurus, Perseus, and Lupus. These particular regions were chosen because they are relatively nearby and large amounts of

supporting data exist. In addition, as pointed out by Myers (1991), these five regions seem to span a wide range of cloud characteristics ("complexity"). We note that our cloud denoted as "Orion" is only part of the overall Orion molecular cloud complex; our region is part of what is generally known as "Orion B", although we refer to the region simply as "Orion" for this paper.

The column density maps were produced from the observed 100μm and 60 μm *IRAS* data by WMD for the Orion, Ophiuchus, Perseus, and Lupus clouds and by Houlahan & Scalo (1992) for the Taurus cloud. Since detailed descriptions of the map producing process are given in the original papers, we present only a brief summary here: The maps begin as flux density matrices, where each pixel of the map is a square with sides of 1 arcminute (notice that this angular size is smaller than the actual satellite resolution, which is estimated to be 2–3 arcminute). After subtraction of background emission, the dust temperature of each pixel is estimated from the observed 60μm/100μm color temperature. After the temperature dependence has been removed from the map, we are left with a map of the 100μm optical depth τ_{100}. The resulting column density maps are shown in Figures 1 – 5.

Our sample of clouds has a fairly large dynamic range, both in spatial extent (typically 400 × 400 pixels) and in column density (e.g., a factor of ~400 in Taurus). Each of these clouds is identified with a known complex of molecular material as mapped in the CO molecule. Notice, however, that the outer boundaries of our clouds are chosen, by necessity, rather arbitrarily. As a result, we can only obtain information about molecular cloud structure on spatial scales smaller than the map size. As a reference point, the physical length scale associated with a 400 arcminute map is ~17.5 pc, for a "standard" distance to the cloud of 150 pc. [†] We can thus study cloud structure over almost two decades in physical scale: ~ 0.1 – 10 pc. This smallest size scale corresponds roughly to the full-width at half maximum (FWHM) contour levels of ammonia cores (e.g., Myers & Benson 1983); this largest size scale samples the "large scale structure" of the molecular clouds.

Since we are using continuum data in this analysis, we avoid the usual problems associated with line emission, where each particular line is subject to different excitation effects. The interpretation of continuum data is thus somewhat cleaner. On the other hand, we have no velocity information in this sample and are therefore confined to studying structure in two spatial dimensions (i.e., in the plane of the sky). As with all maps taken in the plane of the sky, the cloud maps of this paper are subject to projection effects.

One potential problem with these column density maps is that at sufficiently large optical depths (either large A_V or large values of column density), the correlation between τ_{100} and A_V is no longer linear (see Jarrett, Dickman, & Herbst 1989). This effect becomes significant for visual extinctions $A_V > 10$ or so. Of the five clouds considered

[†] The distances to the clouds in Lupus, Taurus, and Ophiuchus are estimated to lie in the range 140 – 160 pc. The distance to Perseus is less well determined but is thought to lie in the range 200 – 350 pc. On the other hand, distance to the Orion cloud is ~400 pc and hence the quoted range of physical scales will be larger by a factor of 8/3 for Orion.

here, only the Orion region has a substantial fraction of its area with A_V larger than this limit. We therefore expect that this problem will not greatly affect our interpretation of the other four clouds. The correction for this calibration problem amounts to a (nonlinear) re-scaling of the maps. Fortunately, under such scaling transformations, the results of our metric-space formalism transform in a simple manner (see Theorems 1 and 2 of AW).

Another potential problem with these column density maps is the possible effects of temperature gradients and multiple temperature components along a single line of sight. These effects have been studied in detail for one particular molecular cloud region (Barnard 5) by Langer et al. (1989). They use a procedure which is similar to the one described above and construct a map of column density from the 60 and 100μm *IRAS* maps. They find that resulting column density map correlates very well with the ^{13}CO map of the same region. However, they find that the normalization of the column density map is wrong in the sense that the estimate of the total cloud mass is different by a factor of 15 from that found using the ^{13}CO data (which is thought to be a good tracer of the mass). Thus, column density maps produced using this method can provide a good tracer of cloud structure but the absolute values of the resulting maps can be problematic (see Langer et al. 1989 for further discussion of these issues).

3. THE FORMAL SYSTEM FOR FORM DESCRIPTION

We utilize a formalism which considers each molecular cloud to be an element of an abstract space X, which corresponds to the space of all possible molecular clouds (see Paper I; see also Elizalde 1987). For a given physical characteristic of interest, this formalism assigns a one-dimensional function (denoted here as an *output function*) to each cloud. The difference between any two clouds can then be determined by finding the difference between their corresponding output functions; this difference, in turn, is measured using a standard distance function (denoted as d) defined on the space of functions (for further discussion of distance functions and metric spaces, see, e.g., Copson 1968). The ordering of a set of clouds is accomplished by assigning a real number – a *coordinate* – to each cloud, where the coordinate is defined to be the distance between the cloud and a well-defined reference state (or set of states). This entire procedure can be depicted schematically as:

$$
\begin{array}{c}
X = \left\{ \sigma \,|\, \sigma \text{ is a cloud} \right\} \\
\Big\downarrow \; d \circ \chi \\
\left(X, d \circ \chi \right) \\
\Big\downarrow \; d \circ \chi|_{\sigma_0} \\
\left\{ \text{coordinate} \right\} \subset \mathbf{R}^+
\end{array}
$$

In the above diagram, we have used the symbol χ to represent the assignment of an output function to a given map. Thus, we begin with the space X of all clouds and we

assign output functions to each cloud. The composition $d \circ \chi$ measures the difference (distance) between clouds by measuring the difference between their output functions (as we discuss below, we take d to be the usual L_2 norm). Using this distance function, we make the original space of clouds into a pseudometric space $(X, d \circ \chi)$. Finally, we assign coordinates (which are positive real numbers) to the maps through the operation denoted as $d \circ \chi\big|_{\sigma_0}$, which measures the distance from the map to the nearest reference map σ_0 (see §3.4). We invoke this procedure for each output function of interest. Further details of this procedure are discussed in Paper I (see also AW). In the following discussion, we describe the output functions that we use for the description and study of molecular clouds.

3.1 Distributions of Density and Volume

One approach to characterizing a molecular cloud to ask how much of the material is at the highest densities. We can define the fraction of the material at high densities in two different ways. We first determine the fraction m of the mass in the cloud (map) at densities higher than a given reference Σ:

$$m(\sigma; \Sigma) \equiv \frac{\int d^n\mathbf{x}\ \sigma(\mathbf{x})\ \Theta\big[\sigma(\mathbf{x}) - \Sigma\big]}{\int d^n\mathbf{x}\ \sigma(\mathbf{x})}, \tag{3.1}$$

where Θ is a step function and where the integrals are taken over the (bounded) domain D of the map. Notice that, for a given map σ, m is a function of one variable (namely Σ). We can also define an analogous function $v(\sigma; \Sigma)$ which measures the fraction of the volume (area in a 2-dimensional map) greater than the reference density Σ:

$$v(\sigma; \Sigma) \equiv \frac{\int d^n\mathbf{x}\ \Theta\big[\sigma(\mathbf{x}) - \Sigma\big]}{\int d^n\mathbf{x}}. \tag{3.2}$$

Given these definitions, we can define a distance between two maps by measuring the difference between their corresponding output functions (using either m or v), i.e., we define a pseudometrics d_m and d_v through

$$d_m(\sigma_A, \sigma_B) = \left[\frac{1}{\langle\Sigma\rangle}\int_0^\infty d\Sigma\,\big|m(\sigma_A; \Sigma) - m(\sigma_B; \Sigma)\big|^2\right]^{1/2}, \tag{3.3}$$

$$d_v(\sigma_A, \sigma_B) = \left[\frac{1}{\langle\Sigma\rangle}\int_0^\infty d\Sigma\,\big|v(\sigma_A; \Sigma) - v(\sigma_B; \Sigma)\big|^2\right]^{1/2}. \tag{3.4}$$

The output functions $m(\sigma; \Sigma)$ and $v(\sigma; \Sigma)$ have another useful interpretation. Let us define $\mathcal{P}_m$ to be (minus) the derivative of the function m with respect to the variable Σ, i.e.,

$$\mathcal{P}_m(\sigma; \Sigma) = -\frac{dm}{d\Sigma} = \frac{\int d^n\mathbf{x}\ \sigma(\mathbf{x})\delta\big[\sigma(\mathbf{x}) - \Sigma\big]}{\int d^n\mathbf{x}\ \sigma(\mathbf{x})}, \tag{3.5}$$

where we have used the fact that the derivative of a step function Θ is a delta function δ. Similarly, we define $\mathcal{P}_v$ via

$$\mathcal{P}_v(\sigma;\Sigma) = -\frac{dv}{d\Sigma} = \frac{\int d^n\mathbf{x}\ \delta\big[\sigma(\mathbf{x}) - \Sigma\big]}{\int d^n\mathbf{x}}\,. \tag{3.6}$$

The quantity $\mathcal{P}_v$ is the probability (per unit surface density) of a point in the map σ having the surface density Σ. Similarly, the quantity $\mathcal{P}_m$ is the probability (weighted by the mass) of a point in the map σ having the surface density Σ. It is straightforward to show that these probability functions are properly normalized, i.e., $\int \mathcal{P}_v d\Sigma = 1$ and $\int \mathcal{P}_m d\Sigma = 1$. The interpretation of the derivatives of m and v as probability distributions greatly facilitates our understanding of how these output functions behave under various transformations (see AW).

3.2 Distribution of Components

We now consider a diagnostic which can discriminate between different geometrical distributions of the high density material. One way to accomplish this goal is to count the number of pieces of the cloud (i.e., topological components) as a function of threshold density Σ (see AW). We first define a reduced space according to

$$X_\Sigma^+ \equiv \Big\{\mathbf{x} \in D \,\Big|\, \sigma(\mathbf{x}) > \Sigma\Big\}. \tag{3.7}$$

For a given threshold density, the space (X_Σ^+, d_E) has a well defined number $n(\sigma;\Sigma)$ of topological components (where d_E is the usual Euclidean metric). We can then define a pseudometric d_n on the space X of all maps through

$$d_n(\sigma_A,\sigma_B) = \left[\frac{1}{\langle\Sigma\rangle}\int_0^\infty d\Sigma\,\big|n(\sigma_A;\Sigma) - n(\sigma_B;\Sigma)\big|^2\right]^{1/2}. \tag{3.8}$$

In defining this distance function, we have chosen to consider where the mass *is* rather than where it *is not*. In other words, we do not explicitly consider holes or voids in the mass distribution.

3.3 Distribution of Filaments

We also require some description which measures the shapes of the pieces of the cloud. Given the breakup of a cloud into components (as described above), we can obtain a measure of the degree to which the components are filamentary (i.e., stringlike). We begin with the usual definition of the diameter $\mathcal{D}$ of a set A, i.e.,

$$\mathcal{D}(A) \equiv \max\Big\{\,|\mathbf{x}-\mathbf{y}| \;\Big|\; \mathbf{x},\mathbf{y} \in A\Big\}. \tag{3.9}$$

For a given threshold density, a molecular cloud map breaks up into components as described in the previous section; each of these components has a well defined diameter. We can also calculate the area $\mathcal{A}$ of a given component. Notice that for a perfectly round

(circular) component, the area and the diameter are related by the obvious relation $\mathcal{A} = \pi\mathcal{D}^2/4$. In order to obtain a measure of the departure of a given component from a circular shape, we first define a factor $\mathcal{F}_j$, which is simply the inverse of the filling factor for a given component, i.e.,

$$\mathcal{F}_j \equiv \frac{\pi\mathcal{D}_j^2}{4\mathcal{A}_j}\,; \tag{3.10}$$

we denote the quantity $\mathcal{F}_j$ as the "filament index" of the jth component. We also define an average factor f:

$$f(\sigma;\Sigma) = \frac{1}{n(\sigma;\Sigma)} \sum_j w_j\,\mathcal{F}_j, \tag{3.11}$$

where the sum is taken over all of the components and where f is explicitly written as a function of threshold density Σ. The quantities w_j are weighting values; we consider both an unweighted version of the filament index ($w_j = 1$) and a weighted version in which each $\mathcal{F}_j$ is weighted by the fraction of material in that component (see AW). A highly filamentary cloud will thus have a very large value of f. On the other hand, our theoretical idealization of molecular clouds breaking up into nearly spherical cores suggests that at sufficiently high threshold density, f should be nearly unity. The pseudometric d_f on the space of clouds then can be written

$$d_f(\sigma_A,\sigma_B) = \left[\frac{1}{\langle\Sigma\rangle}\int_0^\infty d\Sigma\,\left|f(\sigma_A;\Sigma) - f(\sigma_B;\Sigma)\right|^2\right]^{1/2}, \tag{3.12}$$

where f can be either the weighted or unweighted version of the filament function [3.11].

3.4 Assigning Coordinates

In this study, we want to order the set of molecular clouds in a meaningful way. However, a metric (or pseudometric) by itself does not provide a means of ordering a space. In this formal system, we assign "coordinates" (which are simply positive real numbers) to the clouds (maps) by measuring the distance from a given map σ to a reference map σ_0. In this case, we follow Paper I and use uniform density maps ($\sigma_0 = constant$) as reference maps. We also follow Paper I in defining the coordinate to be the distance to the *nearest* uniform density map. Specifically, for a given pseudometric d_χ, we define the coordinate η_χ by

$$\eta_\chi \equiv \min\left\{d_\chi(\sigma,\sigma_0)\,\middle|\,\sigma_0 \text{ is a uniform density map}\right\}. \tag{3.13}$$

See Paper I for further details on implementing this minimization procedure. In any case, the coordinates represent a measure of how far a given cloud is from a uniform state; these coordinates thus provide a measure of the "complexity" of the cloud.

In addition to the coordinates obtained from the output functions described above, we also consider the "self-gravity" of the cloud as an additional coordinate η_w (see AW). Since the maps used in this study are maps of column density (rather than volume

density), the quantity η_w is a two-dimensional measure of "self-gravity" of the cloud. We cannot measure the true (three-dimensional) self-gravity because we do not have full three-dimensional information.

4. QUANTITATIVE RESULTS FOR MOLECULAR CLOUDS

In this section, we use the formal system described above (see also Paper I and AW) to compute output functions and coordinates for the molecular cloud regions in our sample. We thus obtain a quantitative description of these clouds and an overall ordering of their complexity. These results are sufficient to clearly distinguish the clouds in our sample.

4.1 Output Functions

We begin with a discussion of the output functions themselves. The distributions of density $m(\sigma;\Sigma)$ for the clouds are shown in the upper panels of Figures 6–10; the corresponding distributions of volume $v(\sigma;\Sigma)$ are shown by dotted curves in the same figures. Notice that the distribution of density is always greater than the distribution of volume. This result is general and can be shown rigorously for all maps (see Appendix H of AW). In the lower panels of Figures 6 – 10 we show the probability functions $\mathcal{P}_m(\Sigma)$, which represent the probability of a map having the surface density Σ (see equation [3.5]). In the figures, we actually plot $\Delta\sigma\mathcal{P}_m(\Sigma)$, where $\Delta\sigma$ is the estimated uncertainty in the map values. For this paper, we assume that this uncertainaty has a constant value of $\Delta\sigma = 5 \times 10^{-6}$ (Doug Wood, private communication; see also WMD).

The distributions shown in Figures 6 – 10 are generally fairly smooth; in particular, the output functions do not jump suddenly at any given density scale. Notice that a description of cloud structure as high density "clumps" moving through a very diffuse "interclump medium" would produce a very different signature; in the extreme limit, a cloud of this type would show a nearly bimodal distribution in density and hence nearly a step function in $m(\sigma;\Sigma)$, where the step occurs at the threshold of the interclump medium (a second step would occur at the density of the clumps). We thus argue that these clouds exhibit structure that is not adequately described by the simple picture of clumps embedded in an interclump medium ("baseballs in air"). Clumps can still be present, although they must exhibit a range of densities in order to produce the smooth $m(\Sigma)$ profiles observed in these clouds. †

The distributions of topological components $n(\sigma;\Sigma)$ are shown in the upper panels of Figures 11 – 15 and the corresponding distributions of filaments $f(\sigma;\Sigma)$ are shown in lower panels of the same figures. For both of these distributions, we must determine the smallest number of pixels per component that we want to consider as indicative of real structure. Figures 11–15 show the components with 3 or more pixels as the upper solid curve and the components with 9 or more pixels as the lower dashed curve. In the following subsection, we discuss the errors involved in these distributions and the

† Another possibility is that "hard" uniform density clumps exist, but that they are much smaller than the beam size. In this case, the observations are essentially counting the number of clumps per beam and smooth $m(\Sigma)$ profiles can result.

reasoning behind these particular choices. As a reference point, we note that WMD include all components with 7 or more pixels in their sample of "real" cloud structures.

The distributions of components show a great deal of structure but no big surprises. The clouds break up into ~100 separate components and the number varies rapidly (both up and down) with the value of the threshold. These distributions thus provide a quantitative method of showing the generally accepted description of molecular clouds as complex, clumpy, and irregular objects (see, e.g., Blitz 1993; de Geus et al. 1990). The distributions of filaments show that the average value of the filament index over most of the threshold range is $\sim$ 2 to 3. There exists a weak tendency for the filament index to decrease with increasing column density. This trend is expected if gravitational forces (which are intrinsically spherical) play an increasingly larger role at smaller spatial scales (higher column densities).

4.2 Error Considerations

Before we can use the output functions described above to draw conclusions about cloud structure, we must show that the effects of observational uncertainties on our results are sufficiently small. Fortunately, as we discuss below, this formal system allows us to directly address this issue.

As shown in our companion paper AW, the error in the distribution of density $m(\sigma;\Sigma)$ is given by

$$\Delta m = \Delta\sigma \left| \frac{dm}{d\Sigma} \right| , \tag{4.1}$$

where $\Delta\sigma$ is the uncertainty in the original map. We can calculate this uncertainty Δm directly from the output functions themselves. For each cloud, the error Δm reaches a maximum value as a function of the threshold Σ (see Figures 6 – 10). The maximum values are 0.08, 0.012, 0.03, 0.01, and 0.028 for the maps of Lupus, Taurus, Perseus, Ophiuchus, and Orion, respectively. These error estimates represent the *maximum* possible deviation of the distributions $m(\sigma;\Sigma)$ from their true values due to the presence of observational uncertainties in the maps. We thus conclude that the errors in the distributions of density are sufficiently well controlled within this formal system. Similarly, we can show that the errors are also well controlled for the distributions of volume $v(\sigma;\Sigma)$.

We now consider possible errors in the distribution of components function $n(\sigma;\Sigma)$. As discussed in our companion paper AW, spurious components can arise due to pixels in the map erroneously sticking up above the threshold level when the true value of the pixel is below the threshold level. These erroneous pixels can thus produce erroneous "islands" that will be counted as components. To estimate the size of the errors produced by this effect, we must first estimate the probability that a given pixel in the map will be erroneously larger than the threshold level. The calculation of this probability in AW (see their Appendix F) assumes that the errors in the individual pixels are randomly distributed. However, the maps used in this paper are produced from *IRAS* maps which have a 3 arcminute resolution, and yet the final column density maps are given with 1 arcminute pixels. The errors in these maps thus have some correlation, but the functional form of this correlation remains unknown.

To make a start on this problem, we first determine the probability P_1 that a pixel in the map will be erroneously larger than the threshold level for the case of random error distributions. The analysis of AW shows that this probability P_1 is bounded by

$$P_1 < \frac{\sqrt{\pi}}{4} \Delta\sigma \left| \frac{dm}{d\Sigma} \right|_{\max} = \frac{\sqrt{\pi}}{4} \Delta m|_{\max} \tag{4.2}$$

where we have used equation [4.1] in obtaining the second equality. Using the results for Δm given above, we find that the probability P_1 is bounded by 0.035, 0.0053, 0.013, 0.0044, and 0.012 for the maps of Lupus, Taurus, Perseus, Ophiuchus, and Orion, respectively. The maps considered here contain a large number of pixels ($\sim 10^5$) and thus the number of possible erroneous pixels is rather large, 440 – 3500. Consequently, the number of possible spurious components containing only a single pixel is unacceptably large; we therefore remove from consideration all components which consist of only a single pixel. The number of possible spurious components containing two adjacent pixels is $\propto P_1^2$ and is estimated to be in the range $\sim$4 – 250 for the maps in our sample. We also remove two pixel components form consideration. In this study, we keep only those components with three or more pixels. The number of spurious components arising with three or more pixels is $\propto P_1^3$ and is estimated to lie in the range 0.02 – 9. Since this estimate is relatively conservative and since the distributions of components typically have values $\sim$100, we conclude that the errors in the output functions $n(\sigma; \Sigma)$ would be sufficiently well controlled if we consider only those components with 3 or more pixels and if the errors in the pixels were randomly distributed. As a starting point, we thus plot the distributions of components with 3 or more pixels as the solid curves in Figures 11 – 15.

Next, we must consider the possible effects of correlations in the errors. Since the original beam size of *IRAS* is about 3 arcminutes, the correlation length for errors in the maps should not exceed about 3 pixels. Thus, in order to take into account the possible effects of correlated errors, we have calculated separately the number of components with a given number N_P of pixels, for $N_P = 1 - 9$ (note that a component with 9 or more pixels should be larger than the error correlation length in all directions). First, we find that the relative number of components with a small number of pixels (i.e., $N_P = 1, 2, 3$) is small (as expected). † Next, we consider the distributions of components where we include only those components with 9 or more pixels; these distributions are shown as the dashed curves in Figures 11–15. Notice that the general shapes of both the distributions of components and distributions of filaments are roughly the same for $N_{\min} = 3$ and $N_{\min} = 9$ as the minimum number of pixels per component, although the overall number of components for the $N_{\min} = 3$ case is obviously larger. In addition, as we find in the next subsection, the ordering of the clouds for both the components coordinate and the filaments coordinate are independent of $N_{\min}$, where $N_{\min} = 3 - 9$ is the minimum number of pixels per component. Finally, we note that WMD use $N_{\min} = 7$ as the

† Notice that although the bound presented in the previous paragraph allows for hundreds of erroneous pixels, most of these erroneous pixels do not produce spurious components.

minimum number of pixels per component. All of these considerations suggest that the errors in the distributions of components are reasonably well controlled for this case.

For estimating the possible errors in the distribution of filaments function $f(\sigma;\Sigma)$, we use the results of Appendix G in our companion paper AW. The relative uncertainty is approximately given by

$$\frac{\Delta f}{f} \approx \frac{\Delta n}{n}\left\{1 - \frac{f_S}{f}\right\}, \tag{4.3}$$

where f_S is the average filament index of any possible spurious components. As discussed in AW, any spurious components are likely to be composed of relatively few pixels and are thus likely to produce an average filament index f_S which is not far from unity. The term in brackets in equation [4.3] is thus likely to be less than unity. As a result, the relative error in the distribution of filaments function is generally less than that of the component function and hence well controlled for our sample of clouds.

The effect of limited spatial resolution in the original maps leads to loss of information in the output functions. However, the size of this effect is somewhat difficult to determine. In order to consider this issue, we have degraded the spatial resolution of one of our maps (Taurus) and studied the resulting changes in the output functions. This exercise is described in the Appendix.

4.3 Coordinates

Given the output functions shown in Figures 6 – 15, we can calculate coordinates for the maps (see §3.4 and Paper I). The results are shown in Table 1. Large values of the coordinates imply that the cloud is far from a uniform (constant surface density) state; thus, increasing values of the coordinates imply increasing "complexity" of the cloud.

Notice that one should compare different clouds by comparing the relative sizes of a particular type of coordinate. One should *not* compare different types of coordinates for the same cloud because no absolute normalization exists for such a comparison (see the definitions of the coordinates in §3.4; see also Paper I).

For the filament index coordinate, we have included both the weighted and unweighted versions of the output function (see §3.3). Since the weighted and unweighted versions have similar values, the characteristic shape of the components must not depend strongly on the component size (mass).

	η_m	η_v	η_n	η_f	η_{f_w}	η_w
Lupus	1.1	0.8	140	11	15	0.07
Taurus	3.4	2.7	780	49	57	0.06
Ophiuchus	4.7	2.5	260	63	61	0.23
Perseus	2.2	1.8	92	21	19	0.30
Orion	57	1.5	947	312	308	2.08

Table 1. The coordinates for each cloud in the space of maps, based on the distance of the output functions from that of a uniform density map. The coordinates shown here correspond to the output functions for distribution of density (η_m), distribution of volume (η_v), distribution of components (η_n), and distribution of filaments (unweighted η_f, weighted η_{f_w}); the self-gravity coordinate (η_w) is also given.

We now briefly consider the effects of errors on the coordinates. In the previous subsection, we showed that the errors in the output functions are well controlled in this study. In other words, the difference between any of the true molecular cloud maps and the corresponding observed map (with errors) is small when measured with any of pseudometrics in this paper. Theorem 3 of Paper I shows that the difference between the true coordinate (as measured from the "true" map) and the actual observed coordinate (see Table 1) must also be small. The errors in the coordinates are thus also well controlled in this study. This property of the formal system – that small errors in the output functions lead to correspondingly small errors in the coordinates – arises precisely because the formalism is built using metrics (see the proof of Theorem 3 in Paper I for further discussion).

The coordinates given in Table 1 for the distributions of components and the distributions of filaments have been calculated using $N_{\min} = 3$ as the minimum number of pixels per component (i.e., using the solid curves in Figures 11 – 15). If we use $N_{\min} = 9$ as the minimum number of pixels per components (lower dashed curves in Figures 11 – 15), we obtain the new coordinates shown in Table 2 below:

	η_n	η_f	η_{f_w}
Lupus	112	12	16
Taurus	606	49	56
Ophiuchus	176	62	58
Perseus	58	22	19
Orion	571	72	73

Table 2. The coordinates for each cloud in the space of maps, based on the distance of the output functions from that of a uniform density map. The coordinates shown here correspond to the output functions for distribution of components (η_n) and distribution of filaments (unweighted η_f, weighted η_{f_w}), where we have included only those components with 9 or more pixels.

As shown by Table 2, the coordinates for the distributions of components are decreased as we increase the minimum number of pixels per component (compare with

Table 1). However, the ordering of the coordinates for the distributions of components is the same for both the $N_{\rm min} = 3$ (Table 1) and $N_{\rm min} = 9$ (Table 2) cases. On the other hand, the coordinates for the distributions of filaments (both weighted and unweighted) hardly change at all as we increase the minimum number of pixels per component. One exception to this trend is the case of Orion, where a few components with less than 9 pixels persist up to very high intensity values and thus contribute significantly to the coordinate. Notice, however, that the Orion filament index coordinate is still the largest in the sample.

4.4 Ordering the Space of Clouds

Given the coordinates, we can now consider the ordering of the clouds. We note that, in general, any ordering will depend on the physical characteristic being considered. In other words, there is no ***a priori*** reason why the ordering for one coordinate (say η_m) should be the same as that of another (say η_n). However, we find that a relatively well-defined overall ordering for these five clouds does exist. For almost all coordinates given in Table 1, the Orion cloud has by far the largest values. Similarly, the Lupus cloud generally has the smallest values. In addition, the Perseus cloud has coordinate values which are larger than those of Lupus, but smaller than those of the other clouds. The largest ambiguity occurs in the comparison of Taurus and Ophiuchus where Ophiuchus is "greater" in terms of η_m and η_f, but Taurus is "greater" in terms of η_n. Thus, the results of this analysis suggest the overall ordering

$$\text{Lupus} < \text{Perseus} < \text{Taurus} \sim \text{Ophiuchus} < \text{Orion}\,. \qquad (4.4)$$

We note that this ordering is almost the same as the ordering of the total masses of these clouds. We have thus found quantitative evidence for the hypothesis that more massive clouds produce more complicated structures (Myers 1991).

We note that the ordering given by equation [4.4] was obtained by directly calculating the coordinates from the maps shown in Figures 1 – 5. Since the Orion cloud is farther away (by roughly a factor of three) than the other clouds, and since all maps were taken to have roughly the same *angular* size, we could/should rescale the Orion map by a factor $\beta \sim 1/3$. As shown in our companion paper (see Theorem 1 and its Corollary), this rescaling lowers the coordinates for Orion by a factor of $1/\sqrt{3}$. Even with this rescaling, however, Orion is still "greater" than the other clouds in terms of η_m, η_f, η_{fw}, and η_w. The only difference that arises is that Taurus has a larger value of η_n than the rescaled value for Orion. Part of this difference could be due to loss of resolution in Orion. Even under this rescaling, however, the ordering of equation [4.4] still applies. We also note that the Orion map has a larger *area* by a factor of ~9; thus, the number of components *per unit area* in Orion is even smaller by this additional factor (recall that the distribution of components function measures the total number of components, not the number of components per unit area).

The discussion of ordering given above shows that Taurus and Ophiuchus are similar in their coordinates, i.e., the two clouds are approximately the same distance from the nearest uniform state. However, these clouds are still far apart in molecular cloud space (in other words, the clouds are far from identical, as has been stressed many times in the

literature). To be more precise, if we compare the clouds for any output function χ using the distance

$$d_\chi[\chi(\text{Taurus}; \Sigma), \chi(\text{Oph}; \Sigma)], \tag{4.5}$$

we find that the clouds are quite different. We thus emphasize that the condition of two clouds having similar coordinates, $\eta_\chi(\sigma_A) \sim \eta_\chi(\sigma_B)$, is much weaker than the condition that the distance $d_\chi(\sigma_A, \sigma_B)$ between the clouds is small (see Theorem 3 of Paper I).

5. POPULATIONS OF YOUNG STELLAR OBJECTS

In the previous section we presented a quantitative description of the five molecular cloud regions in our sample. In this section, we compare the star formation properties of these same regions. Unfortunately, however, we have no comparable formal system to determine the star formation properties. We will proceed by searching the literature for information concerning the populations of young stellar objects (YSOs) in these five regions. This section is thus, by necessity, less rigorous than the previous one. We note that YSOs can either be deeply embedded infrared sources (Class I in the scheme of Adams, Lada, & Shu 1987) or optically revealed pre-main-sequence stars (Class II or III); we consider both types of YSOs in the following discussion.

We first consider the spectral types of the pre-main-sequence stars found in these molecular cloud regions. We find that Orion contains many more *hot* stars (spectral types O B A F and G) than the Lupus and Taurus clouds (see, e.g., Cohen & Kuhi 1979; Larson 1982; see also Genzel & Stutzki 1989 for a comprehensive review of star formation in Orion). In fact, the Lupus cloud contains almost exclusively M stars (Krautter & Keleman 1987) and thus produces cooler stars than does Taurus. On the basis these population studies of young stellar objects in Orion, Taurus, and Lupus, Myers (1991) argues that the stellar populations obey an ordering of the form

$$\text{Lupus} < \text{Taurus} \ll \text{Orion}. \tag{5.1}$$

We note that this ordering of stellar populations, although somewhat subjective, is consistent with the quantitative ordering of the molecular clouds found in the previous section. The combination of equations [4.4] and [5.1] thus provides quantitative evidence for the hypothesis that more massive stars form in "more complicated" regions (Myers 1991; see also WMD).

The YSO populations of the Taurus and Ophiuchus clouds have been studied and compared by many authors (see, e.g., Wilking & Lada 1983; Wilking, Lada, & Young 1989; Cohen, Emerson, & Beichman 1989; Kenyon et al. 1990; Beichman, Boulanger, & Moshir 1992; and the reviews of Zinnecker et al. 1993 and Lada, Strom, & Myers 1993). These two clouds are roughly comparable in total mass and have approximately the same order of complexity as determined in the previous section (see equation [4.4]). However, the young stellar populations of these two regions seem to have important differences in their luminosity functions. In Ophiuchus, the luminosity function is dominated by embedded (Class I) sources and their number decreases with decreasing luminosity. In Taurus, the luminosity function is dominated by pre-main-sequence (Class II) objects

and their number increases with decreasing luminosity. Although the observed luminosity functions are thus measurably different, the implications for the underlying mass distribution of the YSO populations are difficult to assess due to various selection effects (see the original papers cited above). However, we can tentatively conclude that the YSO populations is these two clouds obey the ordering

$$\text{Taurus} < \text{Ophiuchus}. \tag{5.2}$$

One interesting possibility is that the difference between the YSO populations in these two clouds results from the core region of Ophiuchus containing more luminous sources. In fact, the K-band luminosity function is reportedly different (in the sense of containing brighter sources) in the core region of Ophiuchus than in the outer lying areas of the cloud (Greene & Young 1992; see also Barsony, Schombert, & Kis-Halas 1991; Rieke, Ashok, & Boyle 1989).

For the Perseus molecular cloud complex, a study of the embedded (Class I) populations of YSOs has been recently done by Ladd, Lada, & Myers (1993). This study directly compares the embedded population of Perseus to that of the Taurus molecular cloud. Compared to sources in Taurus, those in Perseus have slightly higher luminosities and distinctly redder (weighted toward longer wavelengths) spectral energy distributions. Both of these characteristics roughly indicate that Perseus is forming stars of higher mass than is Taurus. For the populations of embedded sources in these two clouds, we thus infer that

$$\text{Perseus} > \text{Taurus}. \tag{5.3}$$

This ordering is consistent with recent work (Ladd, Myers, & Goodman 1994) which suggests that NH_3 cores in Perseus have larger mean linewidths than the cores in Taurus. Notice that the ordering [5.3] of the embedded populations is different than the ordering of the overall complexity of the clouds themselves (see equation [4.4]). One possible reason for this discrepancy between the ordering of the clouds and the ordering of the YSO populations is resolution effects. The distance to the Perseus cloud is uncertain, but is thought to lie in the range 200 – 350 pc. If the distance to Perseus is as large as 350 pc, then the map of Perseus has a lower spatial resolution than our map of Taurus. This loss of resolution could make Perseus appear "less complex" in the analysis of previous section.

We note that selection effects can arise in any sample of young stellar objects. In the present case, however, three (and possibly four) of our clouds are approximately the same distance (~150 pc) away and thus the selection effects should be similar. The Orion cloud is farther away (~400 pc) and thus we should not expect to observe the faintest objects in this cloud. However, Orion shows the greatest diversity of young stellar objects and the most evidence for massive star formation; if Orion were closer, these characteristics would be even more apparent. We note, however, that comparisons of both cloud properties and YSO populations are best done among clouds at the same distance in order to minimize differences in resolution effects and selection effects.

To summarize this section, we argue that the populations of young stellar objects in these five molecular cloud regions can be ordered in a manner which is roughly consistent

with the overall ordering of clouds according to "complexity" as determined in the previous section. The YSO population of Orion is unambiguously the "greatest" and that of Lupus is clearly the "smallest". The comparison of Taurus, Perseus, and Ophiuchus is more problematic. The YSO populations of Taurus and Ophiuchus are clearly different, but the sense of the difference is not clear. The Perseus cloud appears to have more luminous (and hence more massive) embedded sources than Taurus, but Taurus is "more complex" according to §4.

Another factor that enters into the relationship between the presently observed structural complexity of clouds and their (current) YSO populations is the *history* of star formation in the cloud. For example, if the clouds have experienced previous episodes of high-mass star formation (Orion and Ophiuchus are likely examples), then the energetic effects of these stars can leave behind substantial signatures of "complexity", even if the stars themselves are no longer present.

We stress that the ordering of YSO populations is presently in an extremely primitive state. As more observational results become available, we can eventually characterize the YSO populations in a given region in terms of a mass function. These mass functions can then be used in a manner analogous to the output functions of the previous section. In particular, we can measure the difference between a given mass function and some standard reference state (e.g., the classic initial mass function of Salpeter 1955). We thus obtain "mass function coordinates" which can be used to order the set of YSO populations in a rigorous manner.

6. SUMMARY AND DISCUSSION

6.1 Results on Cloud Classification

The first result of our analysis is that this method of form description – metric space techniques and output functions – provides a workable classification procedure for molecular cloud maps. For each output function (corresponding to the measurement of some physical quantity), this formalism assigns a coordinate η_χ to each cloud. In this present study, we use five different coordinates and thus assign a 5-dimensional "vector"

$$\eta \equiv (\eta_m, \eta_v, \eta_n, \eta_f, \eta_w) \tag{6.1}$$

to each cloud in our sample. It is clear from examination of Table 1 that this set of coordinates is sufficient to clearly distinguish the clouds in this sample. Thus, this formal system provides a useful framework to classify molecular clouds (see also Paper I and AW). As discussed below (§6.2), this formal system also provides a convenient means of studying cloud properties and structures.

This classification procedure (so far) only includes coordinates describing the internal structure of the clouds. In addition to these coordinates, we can add the obvious additional numbers describing overall clouds properties such as total cloud mass, mean magnetic field strength, mean sound speed, rotation rate, etc. We also note that the particular output functions used here provide a beginning for cloud classification and are

not meant to be definitive. Additional output functions can and should be incorporated into this formal system as our understanding of cloud structure increases.

We find that this set of clouds can be ordered in a meaningful manner (see §4 and especially equation [4.4]). Although the ordering could, in principle, be different for each output function/coordinate used, we find that the ordering of the clouds is roughly consistent for all of the output functions. In addition, the observed ordering (equation [4.4]) roughly confirms the conjecture (suggested by Myers 1991) that the overall complexity of cloud structure increases with the total mass of the complex (see also WMD).

The method of form description used in this work has several advantages. The first advantage is that the observational errors in the output functions (and hence the errors in any results inferred from them) can be well controlled (see §4.2 and AW). We have shown that the errors in the original *IRAS* maps of this study do not produce overly large errors in the output functions we derive from them † Another feature of this formal system is that the results are either invariant under a large class of transformations of the maps, or the results transform in a simple manner (see AW). For the *IRAS* maps used in this study, e.g., the calibration is uncertain at large values of visual extinction A_V (see §2). Fortunately, however, different choices of calibration can be incorporated into our results by a simple rescaling of the output functions (Theorem 2 of AW).

6.2 Results on Cloud Properties

The results of this work show the absence of any preferred column density scale in the output functions. This claim holds for all of the output functions considered. Thus, one result of this study is that, in general, *statements about cloud structure must be made as a function of the density threshold.*

For our sample of clouds, the distributions of density $m(\sigma; \Sigma)$ exhibit very smooth behavior (see Figures 6 – 10); in particular, the functions do not jump suddenly at any threshold level. Thus, we argue that the naive description of clouds consisting of high density "clumps" moving through a diffuse "interclump medium" is insufficient. In the output functions for our observed sample of clouds, no density scales appear to substantiate the existence of a clump density and/or an interclump density.

The observed output functions also show that molecular clouds have a rather large dynamic range in column density. For the clouds in our sample, the ratio of the peak column density to the minimum observable value (the estimated error level in the maps) varies widely but is always quite large. This ratio is approximately 30, 400, 75, 10^3, and 10^5 for Lupus, Taurus, Perseus, Ophiuchus, and Orion, respectively. Although no well developed theory currently exists to describe or predict structure in molecular clouds, the observed large dynamic range in column density in these objects strongly suggests that some highly nonlinear process must be at work. Nonlinear wave motions provide

† We note, however, that in the case of the distribution of components output functions, the possible (unknown) correlations between errors in adjacent pixels make the error analysis difficult for these particular maps.

one possible mechanism to produce this structure (see, e.g., Elmegreen 1990; Adams and Fatuzzo 1993; Adams, Fatuzzo, & Watkins 1994); cloud fragmentation provides a second possible mechanism (e.g., Larson 1985).

The component output functions show rather complicated and nonmonotonic behavior. This finding is consistent with the assertion that the clouds exhibit hierarchical structure, where clumps break up into smaller subclumps as the threshold level is raised (see Houlahan & Scalo 1992). We note, however, that the component output function does not retain information regarding the spatial positions of the components (or clumps). As a result, our results do not directly test for the existence of hierarchical structure. In the future, additional output functions can be developed to address this issue. ‡

The filament output functions provide us with a quantitative measure of how far real molecular clouds are from spherical for each threshold level. Recall that our current theoretical idealization of star forming regions assumes that cloud cores are spherical at high densities; we would thus expect to find $f \rightarrow 1$ at large threshold values. However, as shown in Figures 11–15, the filament index typically has a value in the range 2–3 at large threshold values. We thus obtain a somewhat mixed result: the departure of cloud cores from spherical symmetry occurs at the factor of two level. We note that the smallest size size probed by the maps in this sample is ~ 0.1 pc, roughly the physical size scale of the FWHM contour of an ammonia core (this size scale is small enough to affect protostellar collapse). Notice that the findings of this paper for the shapes of regions in column density maps are roughly consistent with previous determinations of cloud core shapes from various molecular line observations (see, e.g., Myers & Benson 1983; Loren 1989; Myers & Fuller 1992; Myers et al. 1993).

Previous studies of structure in molecular clouds have determined that the cloud boundaries generally exhibit fractal structure (e.g., Bazell & Désert 1988; Dickman, Horvath, & Margulis 1990; Falgarone, Phillips, & Walker 1991). One might naively expect that fractal structures would be highly filamentary and hence would have a rather large filament index (as defined here), and yet the filament index for molecular clouds is not too far from unity. Taken together, these two results imply that while the boundaries of the components (islands) are indeed fractal, most of the interior of the components is "far from the boundary" in the sense that most interior points are not affected by the fractal nature of the boundary. This same state of affairs obtains in the classic example of a fractal boundary – the coastline of Great Britain (Mandelbrot 1977). While the coastline is both fractal and infinite, our British colleagues can walk around freely in the interior without worrying about stepping off the island and into the sea.

We have also considered the populations of young stellar objects in these clouds (§5). As a general rule, the YSO populations obey an "ordering" that is consistent with the ordering of the clouds according to their overall complexity (as given in §4.4). We have thus obtained support for the conjecture that more massive stars tend to form in

‡ Thus far, the methods of Houlahan & Scalo (1992) and those used here are complementary. The former use "data tree" methods which test for the presence of hierarchical structure but do not allow for the construction of metrics (or pseudometrics). As a result, data tree methods cannot be used to order a set of clouds according to their complexity.

more complicated star forming regions. We note, however, that the current data on YSO populations in these clouds are insufficient to make this claim definitive. We also note that not all of the data presented here support this conjecture (see, e.g., equation [5.3]). In the future, as more observational data become available, this question must be studied in more detail. Thus, the important question of bimodal star formation – the assertion that high mass stars form in different environments than low-mass stars – unfortunately remains open. However, significant progress has been made: We now have a quantitative method to describe different star forming environments.

6.3 Future Work

While this present paper provides a preliminary step toward a quantitative description of molecular cloud structure, many directions for future work remain. Larger samples of molecular clouds should be studied and more output functions should be developed (see also AW). As mentioned above, we must also obtain a better understanding of the populations of young stellar objects in these clouds.

One obvious generalization of this work is to study molecular emission line maps of these clouds. Such maps contain velocity information which is not present in the column density maps of this sample. Although the interpretation of the velocity information is not straightforward, a simple method of procedure does exist: Define some type of "Molecular Cloud Hubble Law" which converts the observed line-center velocities into a line-of-sight spatial distance coordinate. One is then left with a density map on a three-dimensional domain and, as described in Paper I, the same (but generalized) output functions can be used. We note that velocity information has often been used to provide a pseudo third dimension for molecular clouds, e.g., in finding clumps and clump mass spectra (see the review of Blitz 1993).

Embedded magnetic fields provide another important component of molecular cloud physics. These fields play an important role in helping to support the clouds against gravitational collapse (e.g., Mouschovias & Spitzer 1976; Shu et al. 1987) and probably also help determine the formation of substructure in these clouds (e.g., Elmegreen 1990, 1993; Adams & Fatuzzo 1993; Fatuzzo & Adams 1993). Polarization maps (which are thought to trace magnetic field structure) of molecular cloud regions are now available (e.g., Goodman 1990). A quantitative analysis of the inferred magnetic field structure should be performed. In particular, the degree to which the magnetic fields lines are tangled (or straight) should be determined.

Finally, we note that a full understanding of molecular clouds must take into account the physical processes which form both the cloud substructure and the clouds themselves. Unfortunately, these processes are not well understood at present (see, e.g., the review of Elmegreen 1993; see also Blitz & Shu 1990). As theories are developed to explain the formation of molecular clouds and their substructure, some method is required to quantitatively describe the resulting structures (both the theoretically predicted structures and the observed structures used to test the predictions). The formal system used here provides a rigorous method to describe such structures and the results of this paper demonstrate the efficacy of this approach.

Acknowledgements

We would like to thank Debbie Daugherty, Pat Houlahan, Phil Myers, John Scalo, and Doug Wood for providing us with processed versions of the *IRAS* maps and for useful discussions. We also would like to thank Peter Barnes, Brian Boonstra, Dick Canary, Marco Fatuzzo, Alyssa Goodman, Paul Ho, Lee Mundy, Greg Thorson, and Rick Watkins for helpful comments and discussions. Finally, we would like to thank the referee – Eugene de Geus – for many useful comments and criticisms. This work was supported by NASA Grant Nos. NAGW–2802 and NAGW–3121, by an NSF Young Investigator Award, and by funds from the Physics Department at the University of Michigan.

APPENDIX: A RESOLUTION STUDY

In this appendix, we discuss the effects of loss of spatial resolution on our results. We choose one of our maps – that of Taurus – for this study. As described in §4, we have already calculated the output functions and the coordinates for this map. We now degrade the resolution of the map by averaging together every four pixels, i.e., we convert the original 400 × 400 map into a 200 × 200 map. This averaging provides a rough approximation to moving the cloud a factor of two farther away and viewing the structure through the same telescope. For this new map, which we denote as Taurus(2), we calculate the output functions and the coordinates as before. We then degrade the resolution a second time by averaging together every four pixels in the Taurus(2) map. We are thus left with a 100 × 100 map which we denote as Taurus(4). For this map, we also calculate the output functions and the coordinates. Finally, we degrade the map yet another time using the same method and denote the resulting map as Taurus (8). The results of this procedure are summarized in Table 3, where we present the coordinates for the four maps of Taurus at differing resolutions.

	η_m	η_v	η_n	η_f	η_{f_w}
Taurus	3.38	2.69	780	49	57
Taurus(2)	3.36	2.69	494	47	54
Taurus(4)	3.31	2.67	267	37	42
Taurus(8)	3.20	2.63	133	25	31

Table 3. The coordinates for the Taurus map at four different spatial resolutions. The coordinates shown here correspond to the output functions for distribution of density (η_m), distribution of volume (η_v), distribution of components (η_n), and distribution of filaments (unweighted η_f, weighted η_{f_w}).

Table 3 shows that the effects of degrading the resolution are not overly severe. The mass fraction and volume fraction coordinates hardly change when we degrade the

resolution by a factor of four. In fact, we must present the coordinates with additional significant figures in order to see the change. The number of components coordinate changes the most; it steadily decreases as the resolution is degraded. This behavior is expected as the telescope beam averages together different pixels in the map (see also §4 where we discuss the issue that the pixel size of the maps is smaller than the original beamsize of the *IRAS* satellite). The filament coordinate does not change substantially when the resolution is degraded by a factor of two, but it begins to decrease when the resolution is degraded by a factor of four. To summarize, loss of resolution tends to make clouds appear "simpler" and the size of this effect is quantified by the coordinates given in Table 3.

REFERENCES

Adams, F. C. 1992, *ApJ*, **387**, 572 (Paper I)

Adams, F. C., & Fatuzzo, M. 1993, *ApJ*, **403**, 142

Adams, F. C., Fatuzzo, M., & Watkins, R. 1994, *ApJ*, in press

Adams, F. C., Lada, C. J., & Shu, F. H. 1987, *ApJ*, **312**, 788

Adams, F. C., & Wiseman, J. J. 1994, submitted to *ApJ* (AW)

Bally, J., Langer, W. D., Stark, A. A., & Wilson, R. W. 1987, *ApJ*, **312**, L45

Barsony, M., Schombert, J. M., & Kis-Halas, K. 1991, *ApJ*, **379**, 221

Bazell, D., & Désert, F. X. 1988, *ApJ*, **333**, 353

Beichman, C. A., Boulanger, F., & Moshir, M. 1992, *ApJ*, **386**, 248

Blitz, L. 1993, in Protostars and Planets III, ed. E. Levy and M. S. Mathews (Tucson: University of Arizona Press), p. 125

Blitz, L., & Shu, F. H. 1980, *ApJ*, **238**, 148

Carr, J. S. 1987, *ApJ*, **323**, 170

Cohen, M., Emerson, J. P., & Beichman, C. A. 1989, *ApJ*, **339**, 455

Cohen, M., and Kuhi, L. V. 1979, *ApJ Suppl.*, **41**, 473

Copson, E. T. 1968, Metric Spaces (London: Cambridge University Press)

Dickman, R. L., Horvath, M. A., & Margulis, M. 1990, *ApJ*, **365**, 586

Elizalde, E. 1987, *J. Math. Phys.*, **28** (12), 2977

Elmegreen, B. G. 1990, *ApJ*, **361**, L77

Elmegreen, B. G. 1993, in Protostars and Planets III, ed. E. Levy and M. S. Mathews (Tucson: University of Arizona Press), p. 97

Falgarone, E., Phillips, T. G., & Walker, C. K. 1991, *ApJ*, **378**, 186

Fatuzzo, M., & Adams, F. C. 1993, *ApJ*, in press

Genzel, R., & Stutzki, J. 1989, *A R A & A*, **27**, 41

de Geus, E. J., Bronfman, L., & Thaddeus, P. 1990, *A & A*, **231**, 137

Goodman, A. A. 1990, PhD Thesis, Harvard University

Gott, J. R., Melott, A. L., & Dickinson, M. 1986, *ApJ*, **306**, 341

Greene, T. P., & Young, E. T. 1992, *ApJ*, **395**, 516

Herbig, G. H. 1962, *Adv. Astron. Astrophys.*, **1**, 47

Houlahan, P., & Scalo, J. M. 1992, *ApJ*, **393**, 172

Jarrett, T. H., Dickman, R. L., & Herbst, W. 1989, *ApJ*, **345**, 881

Kenyon, S. J., Hartmann, L. W., Strom, K. M., & Strom, S. E. 1990, *AJ*, **99**, 869

Krautter, J., & Keleman, J. 1987, *Mitt. Astron. Ges.*, **70**, 397

Lada, C. J., & Shu, F. H. 1990, *Science*, **1111**, 1222

Lada, E. A., Strom, K. M., & Myers, P. C. 1993, in Protostars and Planets III, ed. E. Levy and M. S. Mathews (Tucson: University of Arizona Press), p. 245

Ladd, E. F., Lada, E. A., & Myers, P. C. 1993, *ApJ*, **410**, 168

Ladd, E. F., Myers, P. C., & Goodman, A. A. 1994, *ApJ*, in press

Langer, W. D., Wilson, R. W., Goldsmith, P. F., & Beichman, C. A. 1989, *ApJ*, **337**, 355

Langer, W. D., Wilson, R. W., & Anderson, C. H. 1993, *ApJ*, **408**, L45

Larson, R. B. 1982, *M N R A S*, **200**, 159

Larson, R. B. 1985, *M N R A S*, **214**, 379

Lord, E. A., & Wilson, C. B. 1984, The Mathematical Description of Shape and Form (Sussex: Ellis Horwood)

Loren, R. B. 1989, *ApJ*, **338**, 902

Mandelbrot, B. 1977, The Fractal Geometry of Nature (New York: Freeman)

Mezger, P. G., & Smith, L. F. 1977, in Star Formation (IAU Symposium 75), eds. T. de Jong and A. Maeder (Dordrecht: Reidel), p. 133

Mouschovias, T. Ch., & Spitzer, L. 1976, *ApJ*, **210**, 326

Myers, P. C. 1991, in Fragmentation of Molecular Clouds and Star Formation (IAU Symposium 147), eds. E. Falgarone and G. Duvert (Dordrecht: Kluwer), in press

Myers, P. C., & Benson, P. J. 1983, *ApJ*, **266**, 309

Myers, P. C., & Fuller, G. A. 1992, *ApJ*, **396**, 631

Myers, P. C., & Fuller, G. A., Goodman, A. A., & Benson, P. J. 1991, *ApJ*, **376**, 561

Rieke, G. H., Ashok, N. M., & Boyle, R. P. 1989, *ApJ*, **339**, L71

Salpeter, E. E. 1955, *ApJ*, **121**, 161

Scalo, J. 1990, in Physical Processes in Fragmentation and Star Formation, eds. R. Capuzzo-Dolcetta et al. (Dordrecht: Kluwer), p. 151

Shu, F. H., Adams, F. C., & Lizano, S. 1987, *A R A & A*, **25**, 23

Stenholm, L. G. 1990, *A & A*, **232**, 495

Stutzki, J., & Gusten, R. 1990, *ApJ*, **356**, 513

Veeraraghavan, S., & Fuller, G. A. 1991, in Fragmentation of Molecular Clouds and Star Formation (IAU Symposium 147), eds. E. Falgarone and G. Duvert (Dordrecht: Kluwer), in press

Wilking, B. A., & Lada, C. J. 1983, *ApJ*, **274**, 698

Wilking, B. A., Lada, C. J., & Young, E. T. 1989, *ApJ*, **340**, 823

Williams, J. P., & Blitz, L. 1993, *ApJ*, **405**, L75

Williams, J. P., de Geus, E., & Blitz, L. 1994, *ApJ*, in press

Wood, D. O. S., Myers, P. C., & Daugherty, D. A. 1994, *ApJ Suppl.*, in press (WMD)

Zinnecker, H., McCaughrean, M. J., & Wilking, B. A. 1993, in Protostars and Planets III, ed. E. Levy and M. S. Mathews (Tucson: Univ. of Arizona Press), p. 429

FIGURE CAPTIONS

Figure 1. Column density map of the Lupus molecular cloud region. This map was taken from the results of WMD and is centered on the coordinates R.A. = 15^h 40^m and DEC = -35° 00′ (the map extends 200 minutes of arc in each direction from the center).

Figure 2. Column density map of the Taurus molecular cloud region. This map was taken from the results of Houlahan & Scalo (1992) and is centered on the coordinates R.A. = 04^h 30^m and DEC = 27° 00′ (the map extends 200 minutes of arc in each direction from the center).

Figure 3. Column density map of the Perseus molecular cloud region. This map was taken from the results of WMD and is centered on the coordinates R.A. = 03^h 30^m and DEC = 32° 00′ (the map extends 200 minutes of arc in each direction from the center).

Figure 4. Column density map of the Ophiuchus molecular cloud region. This map was taken from the results of WMD and is centered on the coordinates R.A. = 16^h 25^m and DEC = -24° 00′ (the map extends 200 minutes of arc in each direction from the center).

Figure 5. Column density map of the Orion molecular cloud region. This map was taken from the results of WMD and is centered on the coordinates R.A. = 05^h 47^m and DEC = 00° 00′ (the map extends 200 minutes of arc in each direction from the center).

Figure 6. Upper panel shows the distribution of density [$m(\Sigma)$, solid curve] and distribution of volume [$v(\Sigma)$, dashed curve] output functions for the Lupus cloud. Lower panel shows the corresponding probability distribution $\Delta\sigma\mathcal{P}_m(\Sigma) = -(dm/d\Sigma)\Delta\sigma$; this function represents the probability of a pixel in the map having a value Σ of threshold column density.

Figure 7. Upper panel shows the distribution of density [$m(\Sigma)$, solid curve] and distribution of volume [$v(\Sigma)$, dashed curve] output functions for the Taurus cloud. Lower panel shows the corresponding probability distribution $\Delta\sigma\mathcal{P}_m(\Sigma) = -(dm/d\Sigma)\Delta\sigma$; this function represents the probability of a pixel in the map having a value Σ of threshold column density.

Figure 8. Upper panel shows the distribution of density [$m(\Sigma)$, solid curve] and distribution of volume [$v(\Sigma)$, dashed curve] output functions for the Perseus cloud. Lower panel shows the corresponding probability distribution $\Delta\sigma\mathcal{P}_m(\Sigma) = -(dm/d\Sigma)\Delta\sigma$; this function represents the probability of a pixel in the map having a value Σ of threshold column density.

Figure 9. Upper panel shows the distribution of density [$m(\Sigma)$, solid curve] and distribution of volume [$v(\Sigma)$, dashed curve] output functions for the Ophiuchus cloud. Lower panel shows the corresponding probability distribution $\Delta\sigma\mathcal{P}_m(\Sigma) = -(dm/d\Sigma)\Delta\sigma$; this function represents the probability of a pixel in the map having a value Σ of threshold column density.

Figure 10. Upper panel shows the distribution of density [$m(\Sigma)$, solid curve] and distribution of volume [$v(\Sigma)$, dashed curve] output functions for the Orion region. Lower panel shows the corresponding probability distribution $\Delta\sigma\mathcal{P}_m(\Sigma) = -(dm/d\Sigma)\Delta\sigma$; this function represents the probability of a pixel in the map having a value Σ of threshold column density.

Figure 11. Upper panel shows the distribution of components output function $n(\Sigma)$ for the Lupus cloud (where Σ is the threshold column density). Lower panel shows the corresponding distribution of filaments function $f(\Sigma)$. In both panels, the solid curve shows the distribution which includes all components with 3 or more pixels; the dashed curve shows the distribution which includes only those components with 9 or more pixels.

Figure 12. Upper panel shows the distribution of components output function $n(\Sigma)$ for the Taurus cloud (where Σ is the threshold column density). Lower panel shows the corresponding distribution of filaments function $f(\Sigma)$. In both panels, the solid curve shows the distribution which includes all components with 3 or more pixels; the dashed curve shows the distribution which includes only those components with 9 or more pixels.

Figure 13. Upper panel shows the distribution of components output function $n(\Sigma)$ for the Perseus cloud (where Σ is the threshold column density). Lower panel shows the corresponding distribution of filaments function $f(\Sigma)$. In both panels, the solid curve shows the distribution which includes all components with 3 or more pixels; the dashed curve shows the distribution which includes only those components with 9 or more pixels.

Figure 14. Upper panel shows the distribution of components output function $n(\Sigma)$ for the Ophiuchus cloud (where Σ is the threshold column density). Lower panel shows the corresponding distribution of filaments function $f(\Sigma)$. In both panels, the solid curve shows the distribution which includes all components with 3 or more pixels; the dashed curve shows the distribution which includes only those components with 9 or more pixels.

Figure 15. Upper panel shows the distribution of components output function $n(\Sigma)$ for the Orion region (where Σ is the threshold column density). Lower panel shows the corresponding distribution of filaments function $f(\Sigma)$. In both panels, the solid curve shows the distribution which includes all components with 3 or more pixels; the dashed curve shows the distribution which includes only those components with 9 or more pixels.

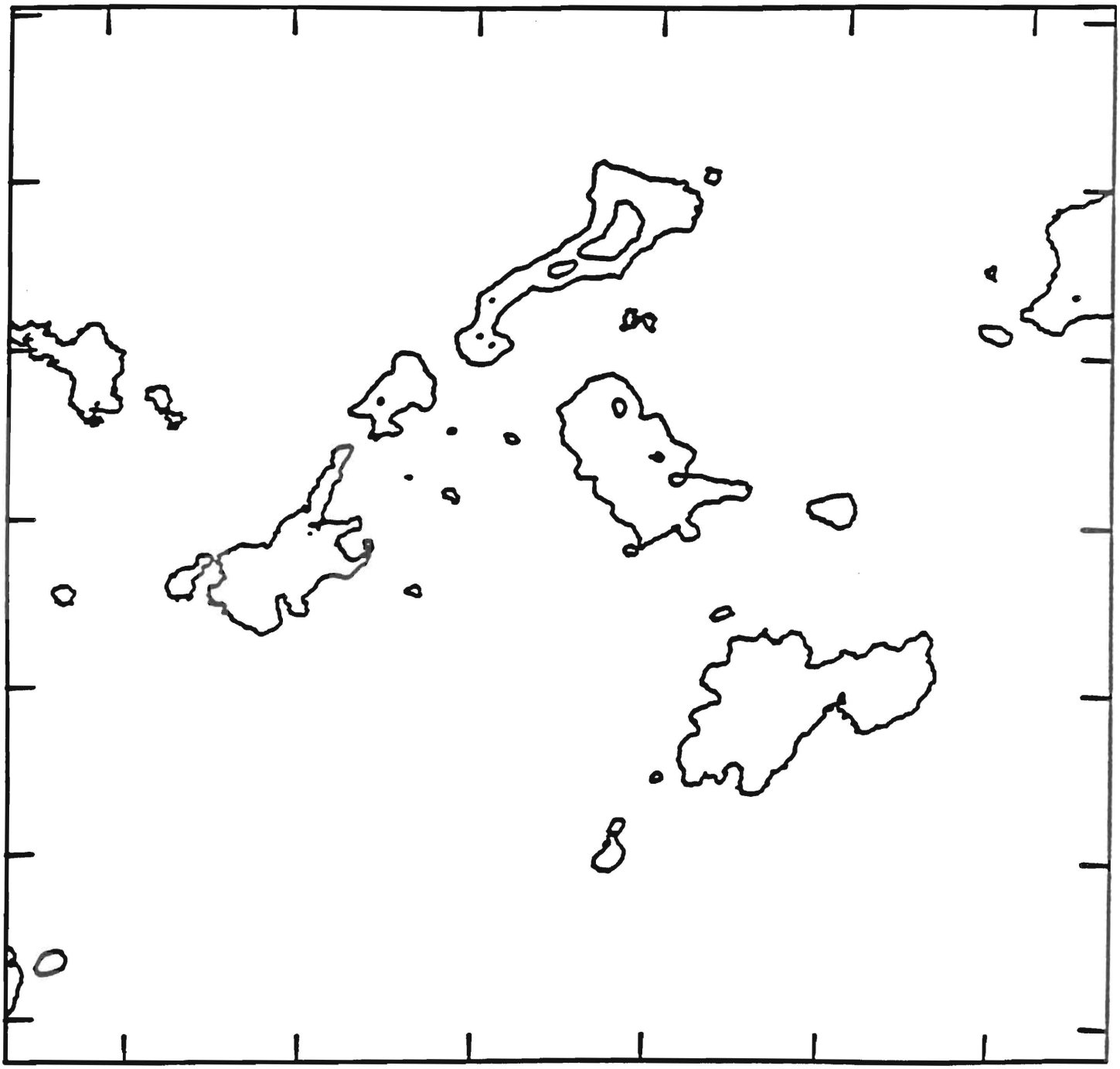

Fig. 1 Lupus

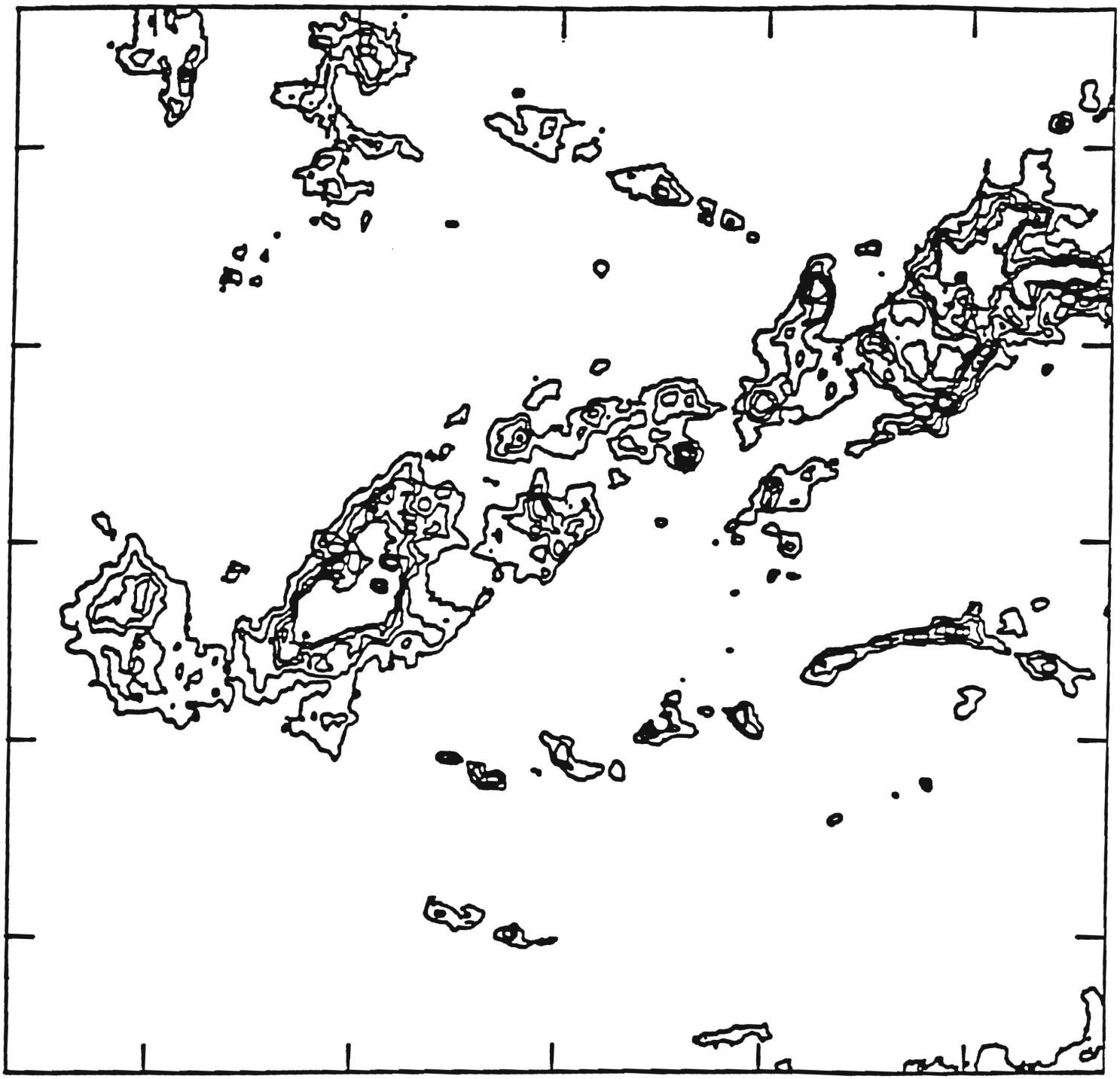

Fig. 2 TAURUS

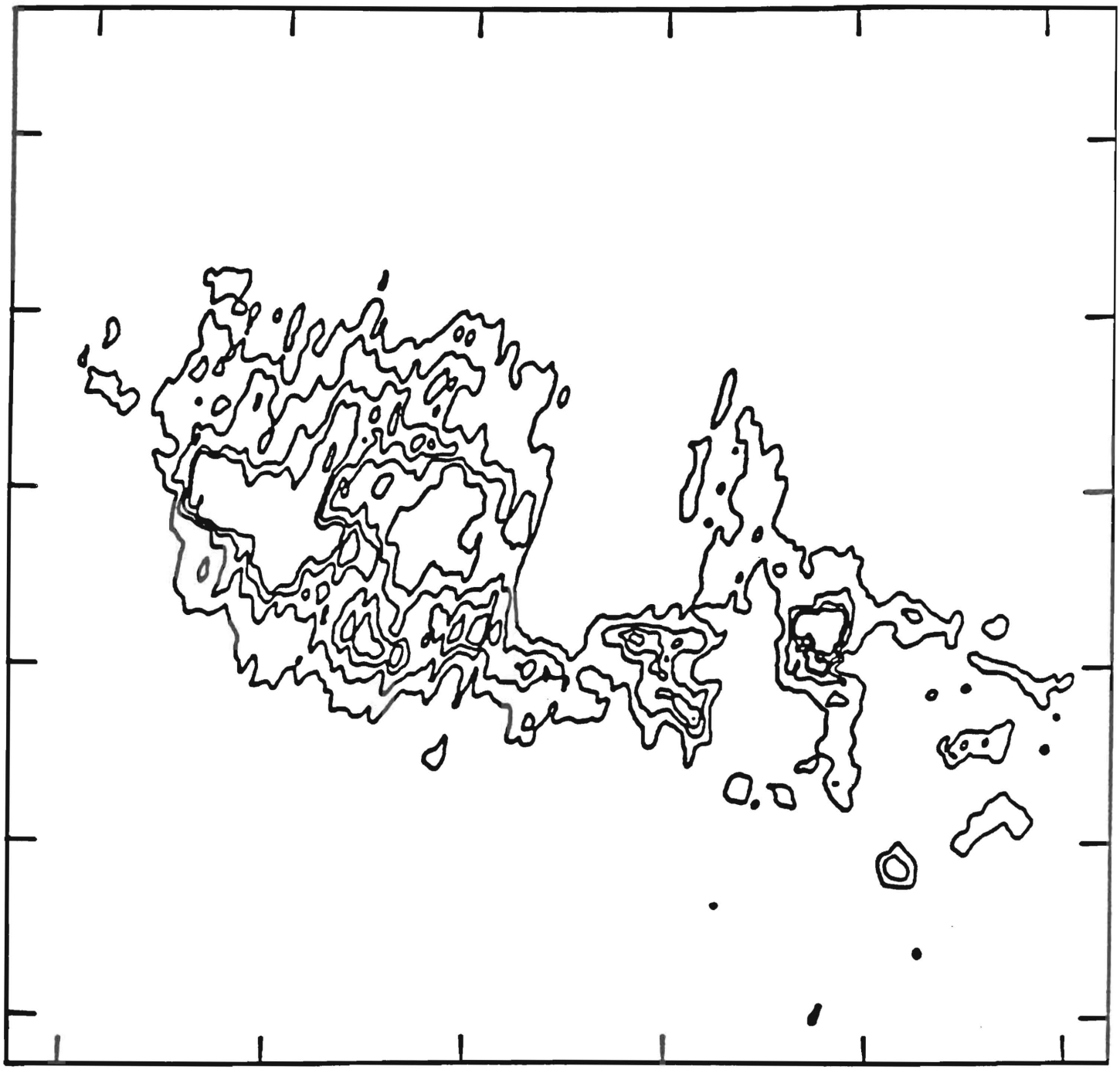

Fig. 3 PERSEUS

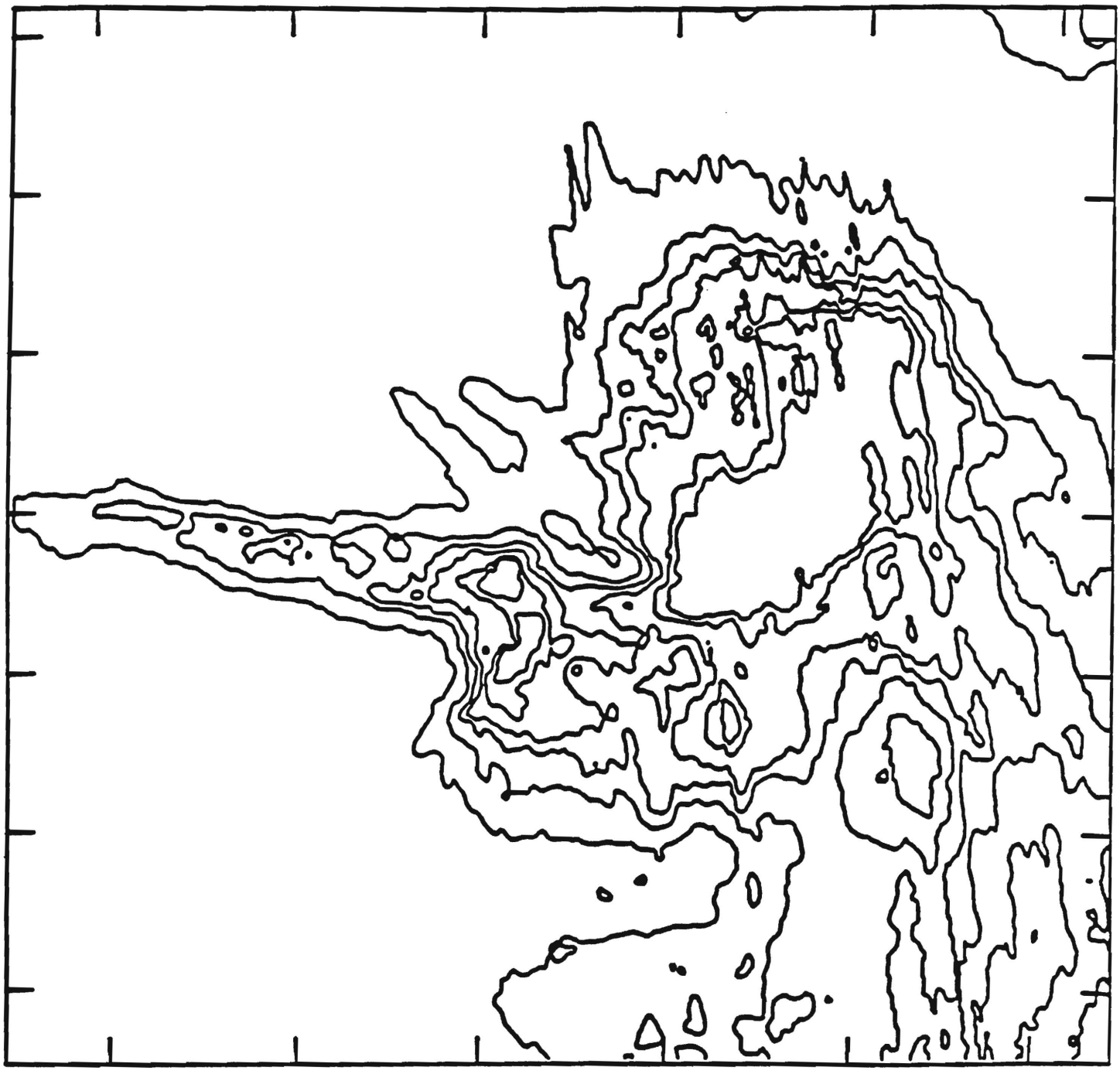

Fig. 4 OPHIUCHUS

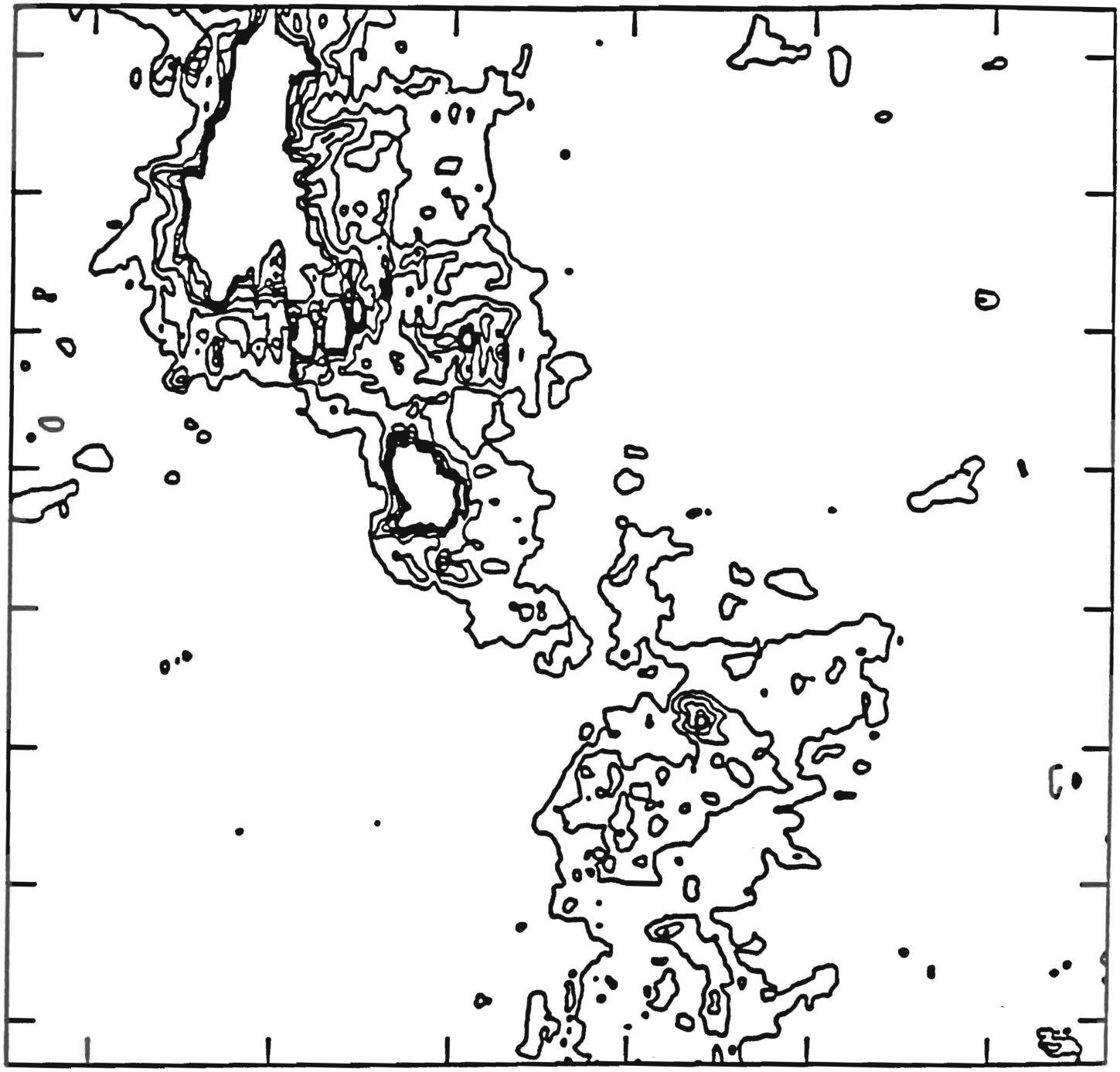

Fig. 5 ORION

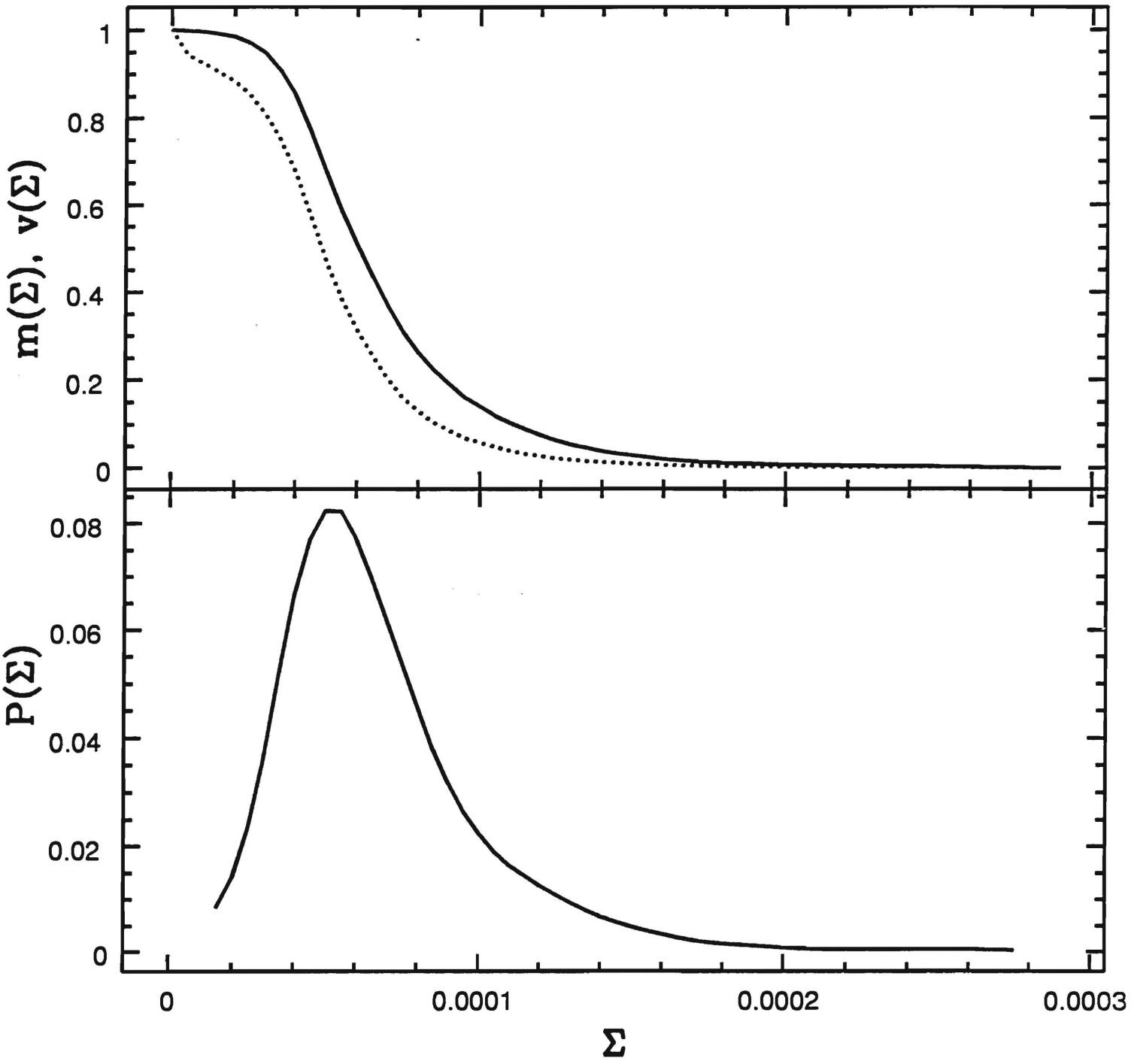

Fig. 6 Lupus

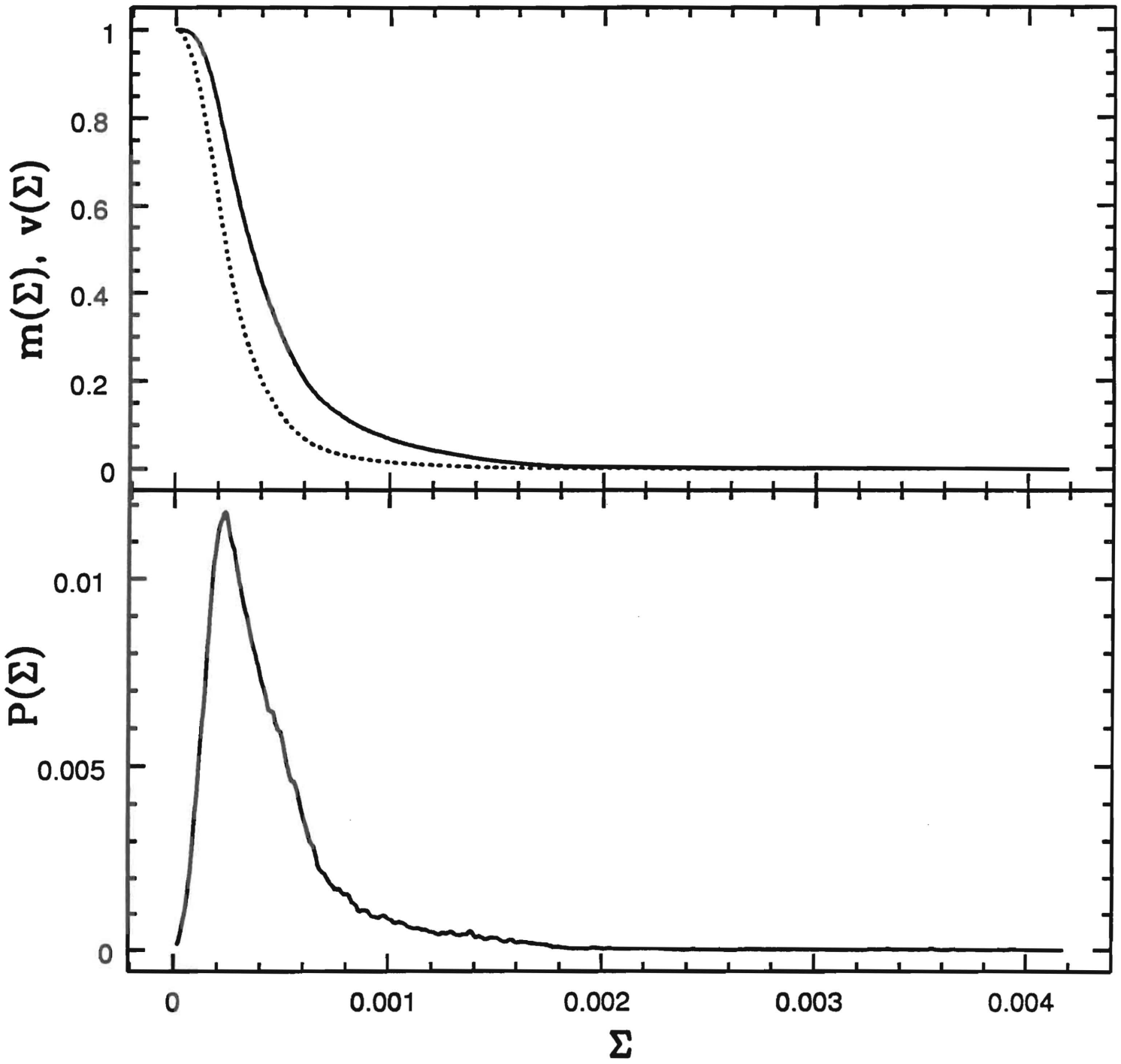

Fig. 7 TAURUS

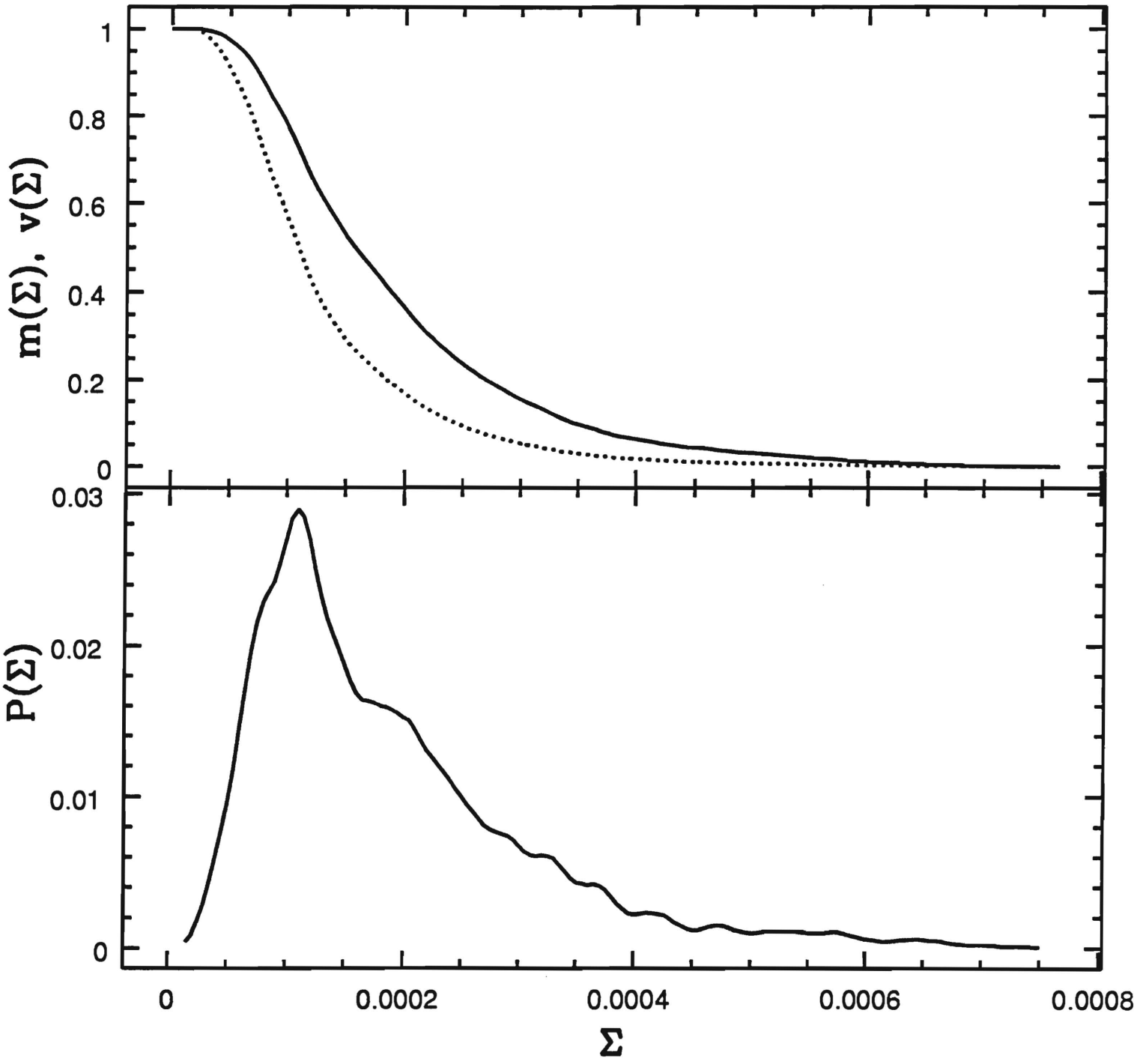

Fig. 8 PERSEUS

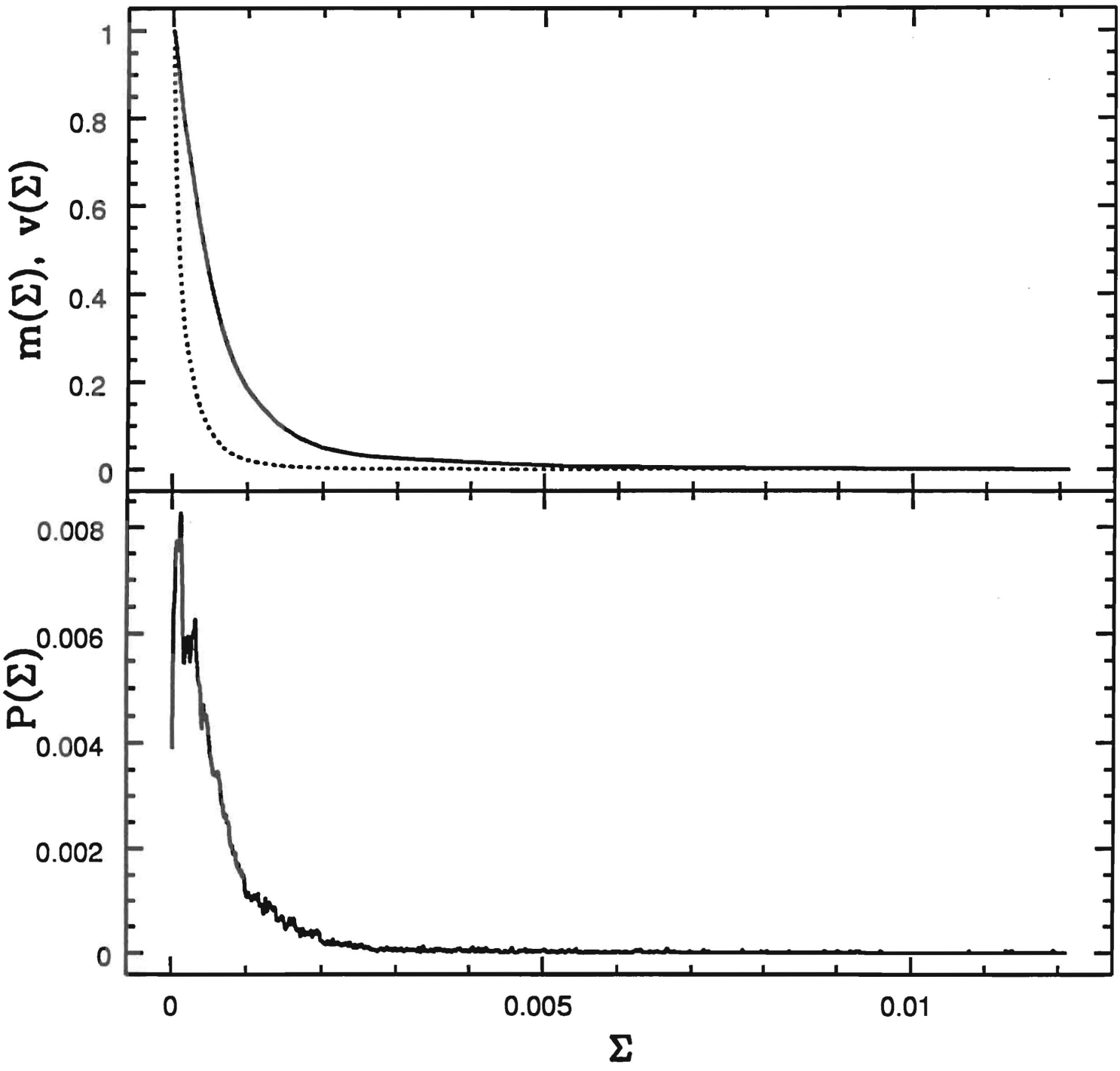

Fig. 9 OPHIUCHUS

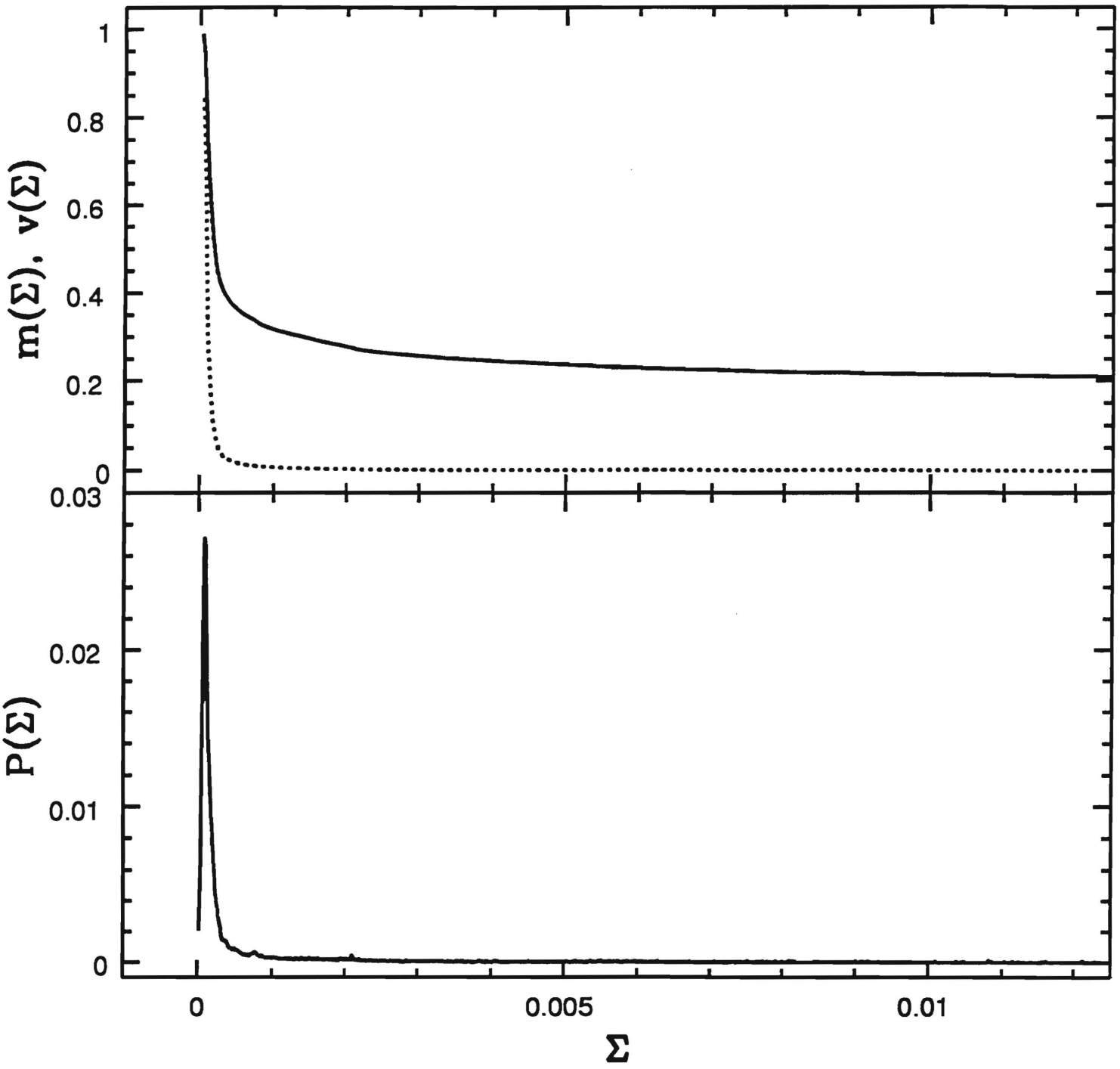

Fig. 10 ORION

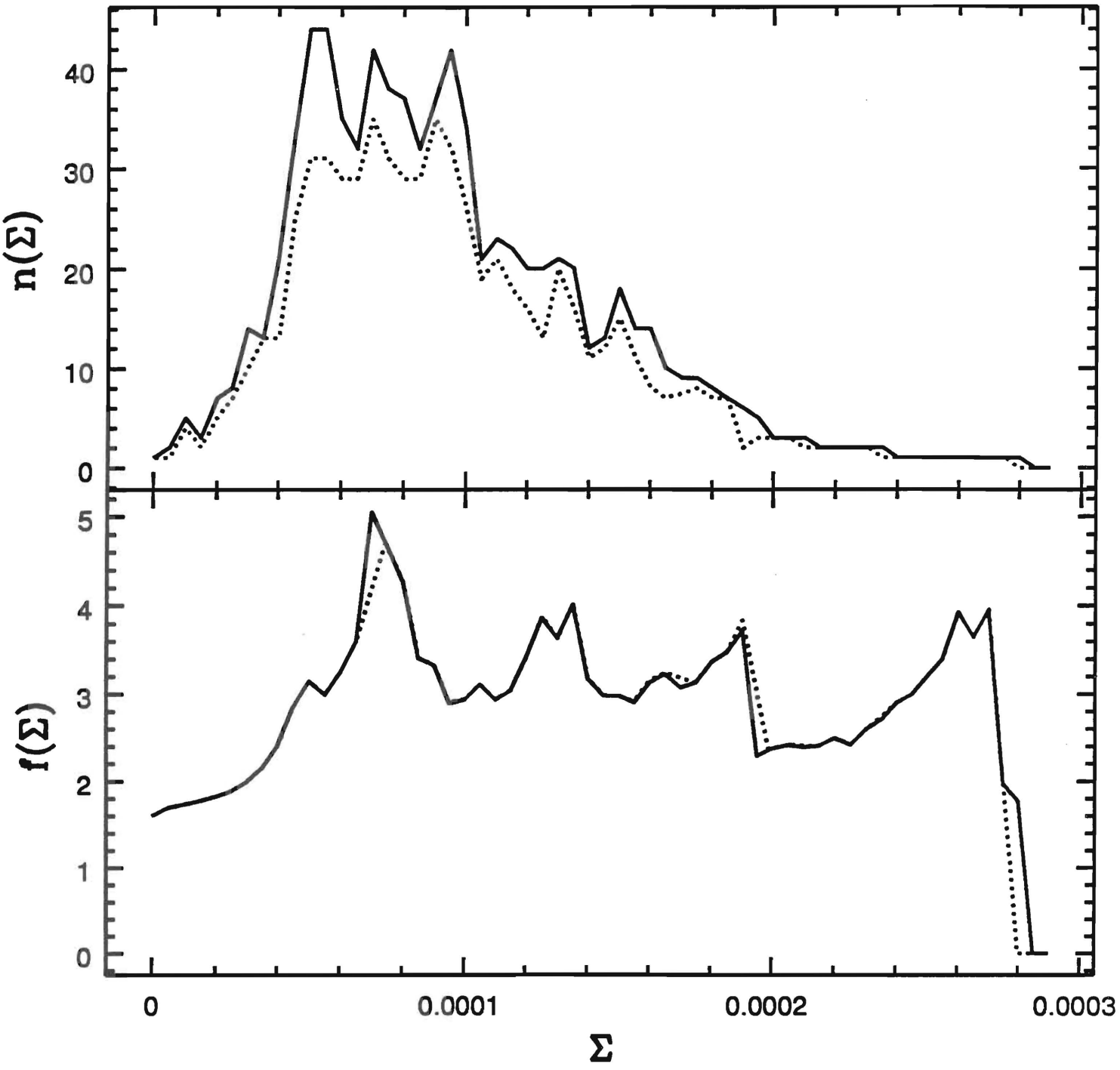

Fig. 11 Lupus

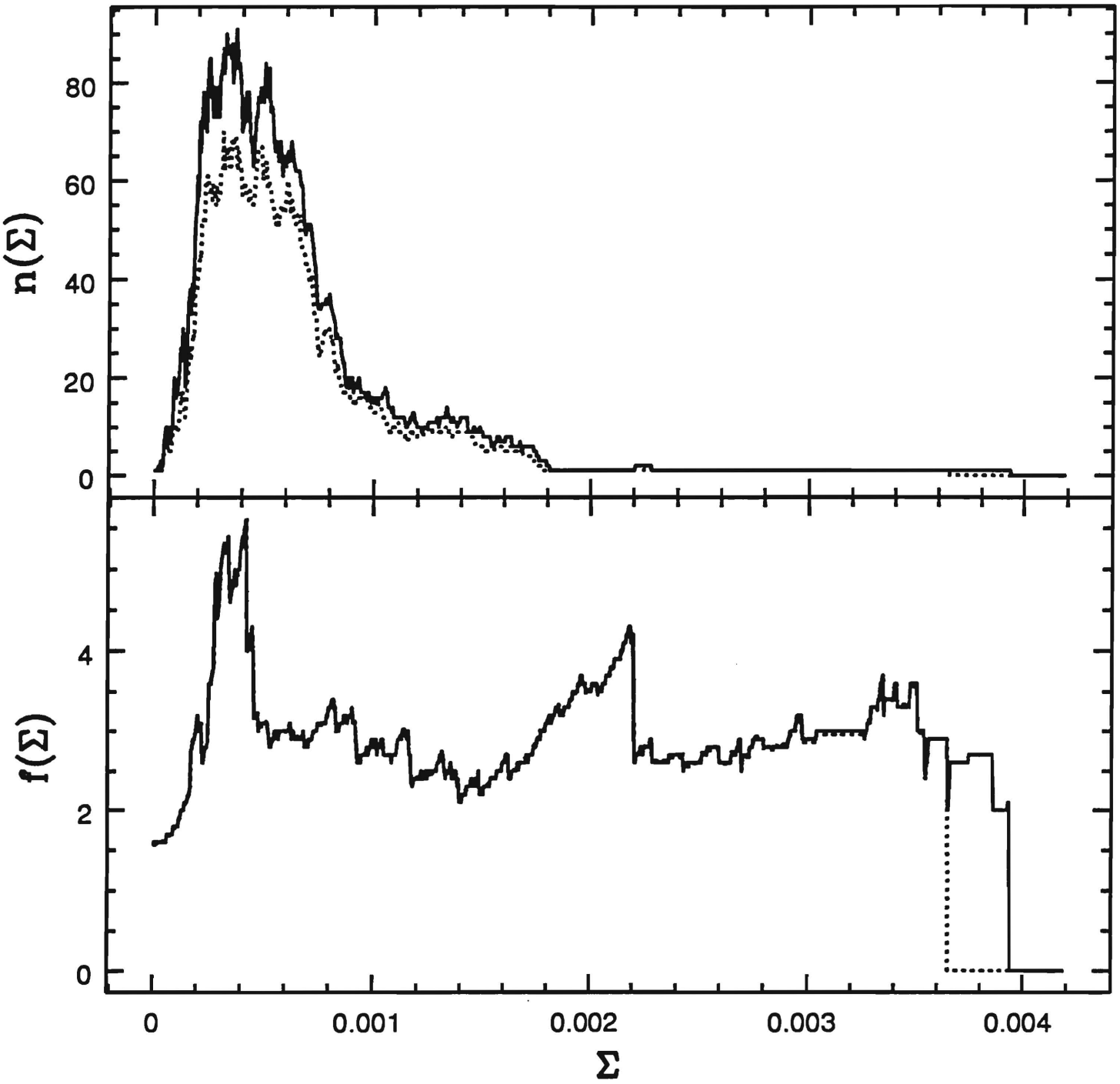

Fig. 12 TAURUS

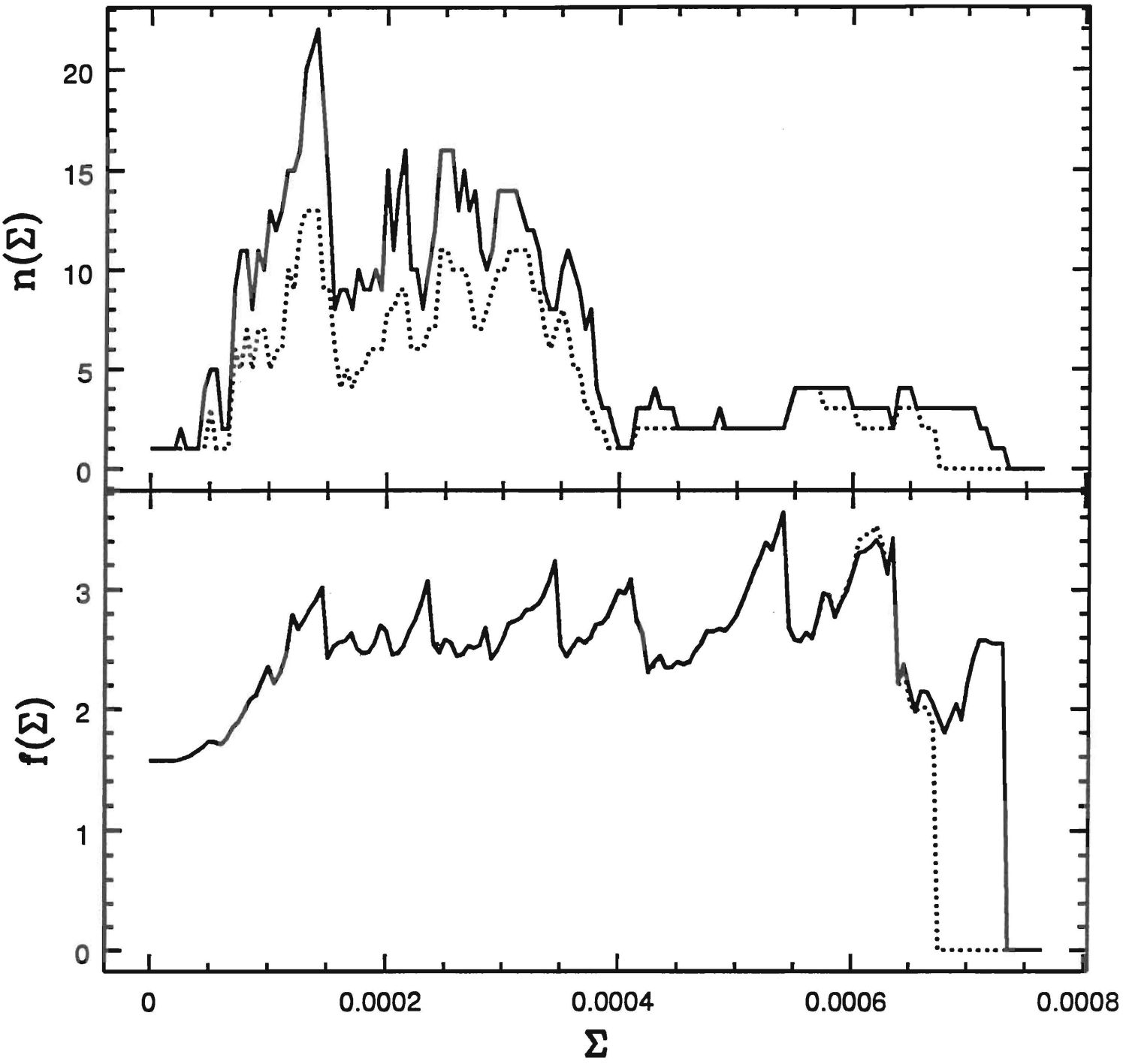

Fig. 13 PERSEUS

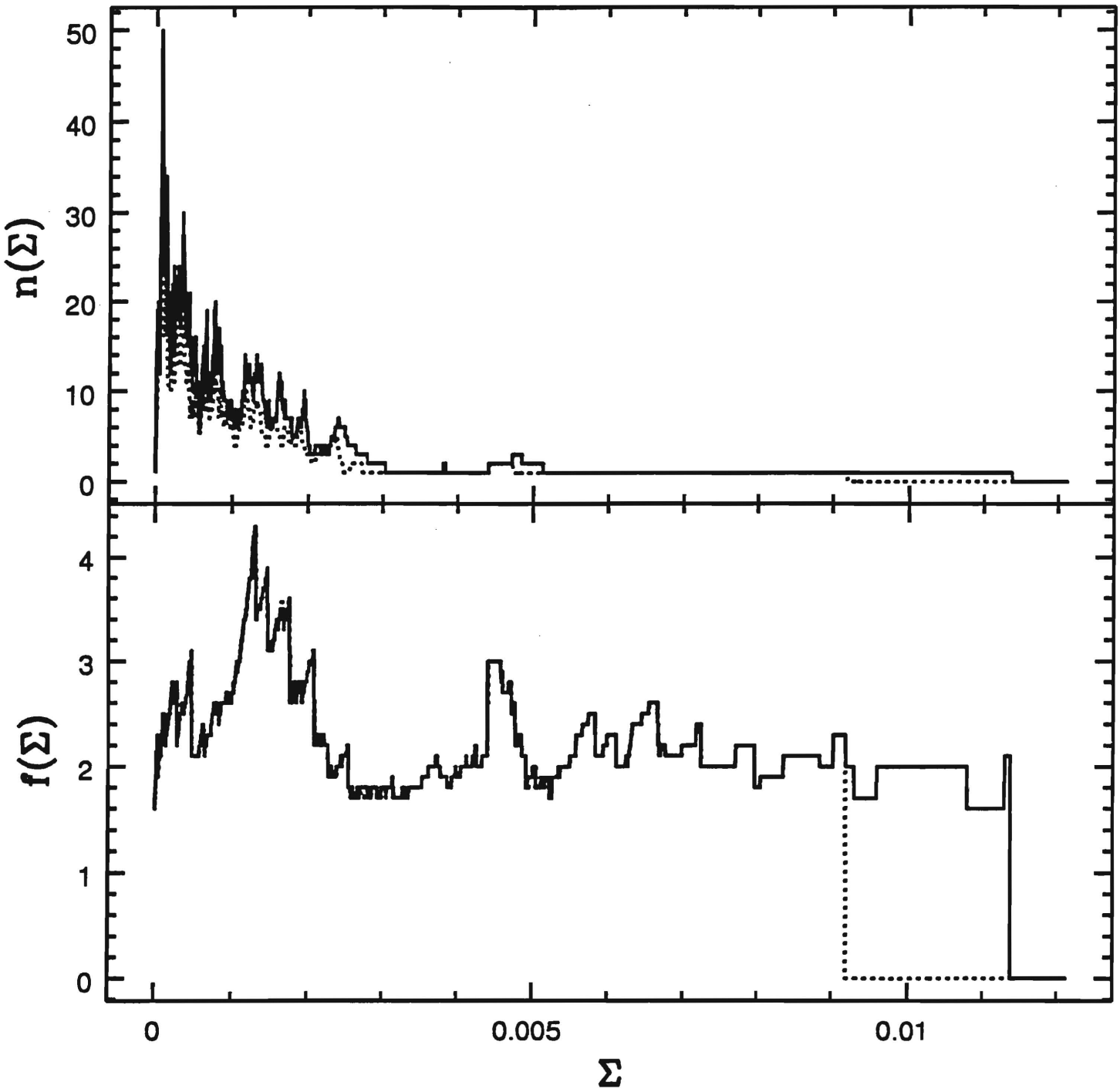

Fig. 14 OPHIUCHUS

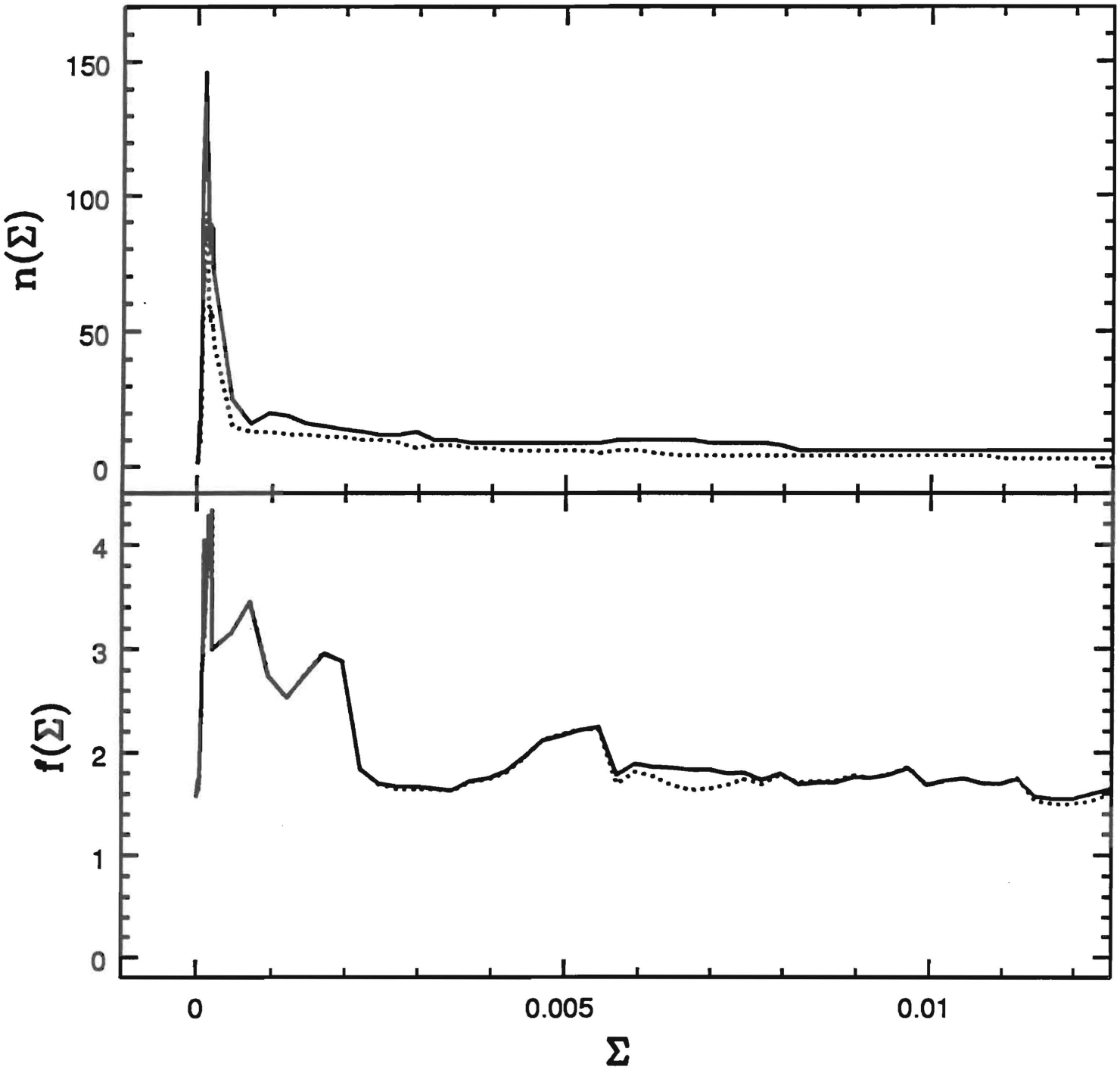

Fig. 15 ORION